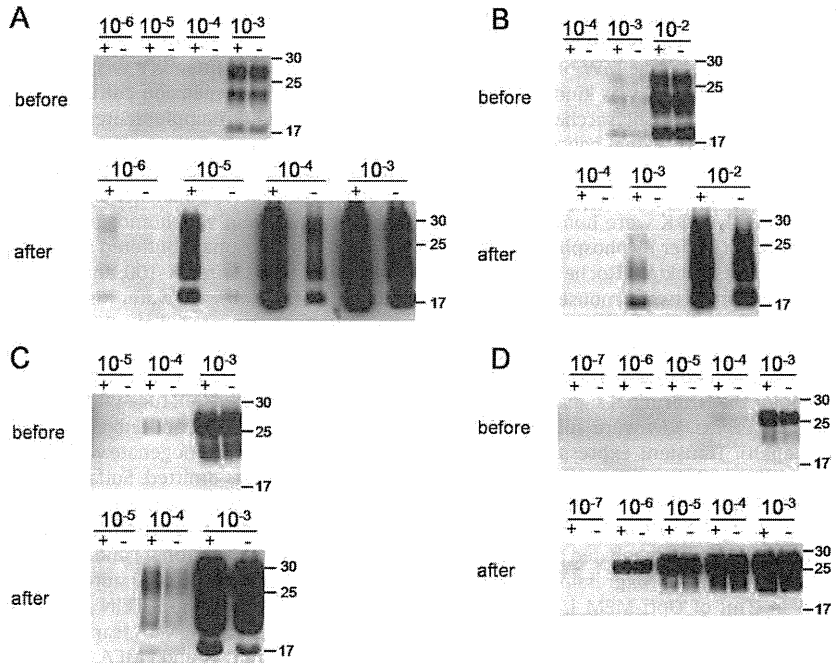

Fig. 2. Comparison of the effect of low molecular weight heparin on the PMCA efficiency of vCJD, sCJD, and 263 K. Western blotting of PrP^{res} before and after the PMCA is shown. Combinations of seed and substrate are vCJD with cell lysate as a substrate (A), sCJD with cell lysate (B), 263 K with cell lysate (C), and 263 K with brain homogenate (D). Representative experiments are shown. Positions of molecular weight markers in kDa are indicated at the right of each panel. Dilution factors of seed in powers of 10 are indicated at the top of each panel. + or − indicates with and without heparin, respectively. "before" indicates samples before PMCA, and "after" indicates those after PMCA.

2 reasons for this variability were speculated to be dilution errors, which occur during dilution of aggregated materials such as brain homogenate, and variability in amplification itself. Thus, duplicates or triplicates of samples were tested simultaneously. Dextran sulfate (average MW, 1400 kDa) moderately enhanced PMCA efficiency (Fig. 1A, left side). The maximum effect was observed at a concentration of 5 mg ml^{-1}; effects were reduced at higher and lower concentrations. However, dextran sulfate (average MW, 8 kDa) showed no enhancing effect (Fig. 1A, right side). This indicated that the effect of dextran sulfate depends on its molecular weight and that 8 kDa, which is equivalent to approximately 25 saccharides, is insufficient to exert an effect. Both LMW (average MW, 4–6 kDa) and HMW (average MW, 13–17 kDa) heparin greatly enhanced PMCA efficiency (Fig. 1B). Optimal concentrations of both LMW and HMW heparin were 100 μg ml^{-1}, and enhancing effects decreased drastically at 10× or 1/10th the optimal concentration. Enhancing effects of LMW heparin were confirmed using two other vCJD brain obtained from different patients (data not shown). Fondaparinux, a sulfated pentasaccharide of approximately 1.7 kDa that is a synthetic heparin analog, had no enhancing effect (Fig. 1C), indicating that the effect of heparin also depends on its molecular weight. Dermatan sulfate greatly enhanced PMCA efficiency at concentrations of 0.1–10 mg ml^{-1} (Fig. 1D). PPS inhibited PMCA efficiency in a dose-dependent manner (Fig. 1E). Because it was possible that the optimal concentration ranges of PPS was very narrow, we performed tests using concentrations with half-log increments, but did not observe enhancing effects (data not shown). To compare enhancing effect between additives, we densitometrically analyzed chemiluminescent intensities. Enhancing factors were calculated as ratios of intensities with additives at optimal concentrations and without additives. Enhancing factors of LMW heparin, HMW heparin, and dermatan sulfate were comparable, of approximately 30-, approximately 30-, and more than 20-fold, respectively. Dextran sulfate had a lower enhancing effect, of approximately 8-fold. LMW heparin was used for the following experiments.

The effect of heparin on cell-PMCA of vCJD, sCJD, and 263 K was studied. Serial 10-fold dilutions of vCJD seed were prepared, PMCA was performed in the presence or absence of 100 μg ml^{-1} LMW heparin, and the signal intensities of PrP^{res} before and after PMCA were compared by western blotting (Fig. 2A). Before PMCA, PrP^{res} signals were detected from a 10^{-4} dilution of the seed. After PMCA, signals amplified from $\geq 10^{-6}$ dilution of seed were detected with heparin, whereas signals amplified from $\geq 10^{-5}$ dilution of seed were detected without heparin, indicating that amplification efficiency was approximately 100-fold or 10-fold per round of PMCA with or without heparin, respectively.

The effect of heparin on the cell-PMCA of sCJD was studied in a similar manner (Fig. 2B), except that 1 mg ml^{-1} heparin was used, because this concentration was optimal (data not shown). Signal intensities of PrP^{res} after PMCA with heparin were stronger than those without heparin by a magnitude of less than a few fold.

The effect of heparin on PMCA of 263 K was studied in cell-PMCA and PMCA by using brain homogenate as a substrate. Because the optimal concentration for 263 K was ambiguous (data not shown), heparin concentrations of 100 μg ml^{-1} and 1 μg ml^{-1} were used for cell-PMCA and PMCA with brain homogenate, respectively. In cell-PMCA, signal intensities of PrP^{res} after PMCA with heparin were comparable to or slightly stronger than those without heparin (Fig. 2C). In PMCA with brain homogenate, signal intensities of PrP^{res} after PMCA with and without heparin were virtually identical, indicating that heparin had no effect (Fig. 2D). Therefore, the effect of heparin on cell-PMCA was seed dependent.

The enhancing effect of heparin on multi-round cell-PMCA of vCJD was studied. Three series of serial 100-fold dilutions were prepared independently and subjected to multi-round cell-PMCA with and without heparin. Amplified PrP^{res} at each round was detected by western blotting (Fig. 3 and Fig. S2). All 3 replicates for 10^{-8} and 10^{-10} dilutions generated signals in PMCA with heparin by the third or sixth round, respectively, whereas all 3 replicates for 10^{-8} dilutions generated signals in PMCA without heparin at the

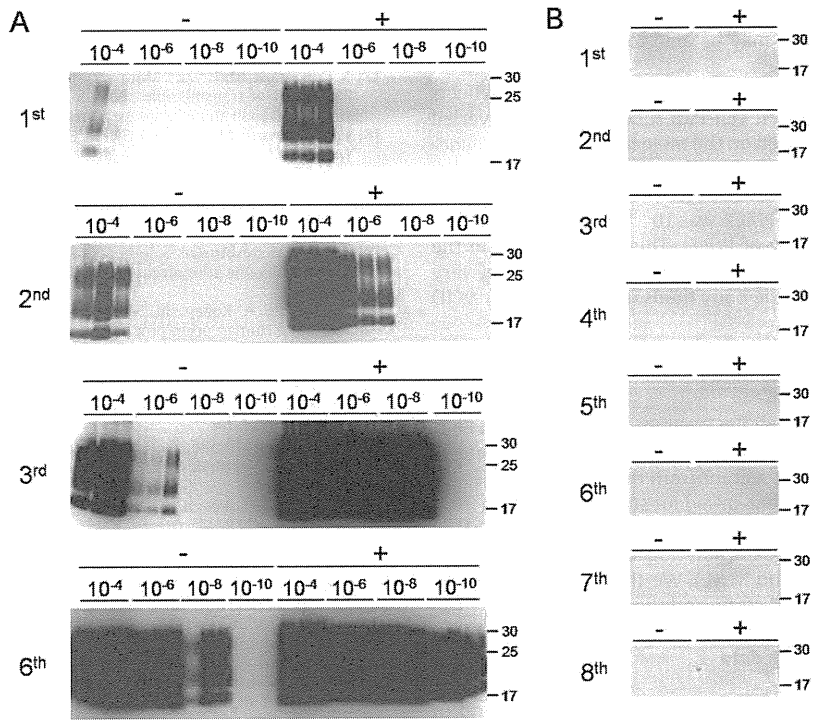

Fig. 3. Multi-round cell-PMCA of vCJD with and without heparin. Western blotting of PrP^{res} after each round of PMCA with vCJD seed (A) and with no seed (B) is shown. Round numbers are indicated at the left of each panel. Positions of molecular weight markers in kDa are indicated at the right of each panel. Dilution factors of seed in powers of 10 are indicated above each panel. + or − indicates with and without heparin, respectively.

sixth round (Fig. 3A and Fig. S2). In another experiment, 3 of 6 replicates for 10^{-10} dilutions generated signals by the sixth round (data not shown). The amount of PrP^{res} in 100 μl of 10^{-10} dilution of vCJD brain was estimated to be approximately 0.5 fg (data not shown). Therefore, we concluded that the detection limit of vCJD by cell-PMCA with heparin is 10^{-10} dilution of brain or 0.5 fg of PrP^{res}. Signals for 10^{-8}dilutions with heparin appeared 3 rounds earlier than those without heparin. Decreasing the number of PMCA rounds required to detect signals is useful to save time and to reduce the chance of PrP^{res} contamination. In cell-PMCA with heparin, round numbers showed linear correlation with dilution factors up to the third round. As a negative control, 6 and 10 replicates of substrates containing no seed without or with heparin, respectively, were subjected to multi-round cell-PMCA simultaneously. No signals appeared at least up to the eighth round (Fig. 3B). Thus, we believe that no *de novo* generation of PrP^{res} occurred under these conditions.

We studied effects of various sulfated polysaccharides on cell-PMCA of vCJD. We found that heparin enhanced the amplification efficiency of cell-PMCA of vCJD to the extent of more than 100-fold per round and that the enhancing effects of heparin depended on prion strains. The mechanism behind the enhancing effect of heparin is unclear. Heparin is known to bind PrP^{C} [9]; thus, it may provide scaffolds resulting in concentrating substrates [22]. Heparin exerted effects at a relatively narrow range of concentrations. The reason for the existence of an optimal concentration remains unclear.

The effect of each sulfated polysaccharide on *in vitro* amplification efficiency varied among prion strains. The extent of the enhancing effect of heparin differed between vCJD and sCJD (Fig. 2A and B). The only difference in their PMCA conditions was attributable to the seeds. The genotype of PrP in these seeds was 129M/M. Thus, the reason for the different effects between the 2 types of Creutzfeldt–Jakob disease seems to be related to the structure of PrP^{Sc}, for example types 1 and 2 [17]; to factors associated with PrP^{Sc}; or to factors in the individual brains. The effect of heparin on PMCA of 263 K also differed from that of vCJD. When cell lysate was used, it is possible that endogenous human PrP^{C} expressed in 293F cells caused heterogeneous inhibition as observed in heterozygote [11]. When brain homogenate was used, either other cofactors for PMCA were depleted because of the very large amplification, resulting in a block of further propagation, or brain homogenate contained heparin analogs in excess of the optimal concentration.

Heparan sulfate enhanced the conversion efficiency of 263 K in a cell-free conversion assay when purified PrP^{C} was used as a substrate [22]. Reasons for the discrepancy to our data could be differences in the concentration of endogenous heparin or its surrogates in substrates, differences between heparin and heparan sulfate, or differences in the mechanisms of propagation.

PPS strongly enhanced PMCA of BSE [16] but showed inhibitory effects on the PMCA of vCJD (Fig. 1E). This discrepancy is surprising because vCJD is derived from BSE and PrP^{Sc} of vCJD seems to have a biological character similar to PrP^{Sc} of BSE [2,5,10]. Reasons for the difference in the PPS effect may be related to sequence differences of PrP and/or other factor(s) present in the seed or substrates.

The sensitivity of heparin-assisted cell-PMCA for vCJD was 10^{-10} dilution of brain or 0.5 fg of PrP^{res}. This sensitivity seems to be comparable to that of other methods, as has been recently reported [1,8]. Given this level of sensitivity, it seems possible to detect PrP^{res} from clinical specimens, especially from body fluids of asymptomatic vCJD patients. Overall amplification in cell-PMCA of 263 K was highly inferior to that in the PMCA with brain homogenate. We speculate that the reasons for this are the heterogeneous inhibition described previously, the lack of a hamster background in human-derived cells, and/or the lack of brain-derived factor(s) in

kidney-derived cells. If brain-derived factors are critical, the human counterparts of such factors may be able to further enhance the cell-PMCA efficiency of vCJD.

In conclusion, we investigated for the first time the effects of sulfated polysaccharides on cell-PMCA of vCJD. Effects varied among additives and depended on the molecular weights. Enhancing effects of heparin varied among prion strains: the effects were high in vCJD, little or negligible in sCJD and 263 K. The detection limit of heparin-assisted cell-PMCA was 10^{-10} dilutions of the vCJD brain or approximately 0.5 fg of PrP^{res}. This improvement in the PMCA of vCJD is a significant step toward the detection of very minute amounts of PrP^{Sc} in the body fluids of asymptomatic vCJD patients.

Acknowledgements

This study was supported by the Program for Promotion of Fundamental Studies in Health Sciences of the National Institute of Biomedical Innovation (T.K.); a grant from the Ministry of Health, Labor and Welfare (T.K.); a grant-in-aid for scientific research from the Ministry of Education, Culture, Sports, Science and Technology (T.K. and A.T.); and the Benesis Corporation and Mitsubishi Tanabe Pharmaceutical (T.Y., M.Y., and M.M.). We thank Prof. K. Doh-ura for kindly providing the 263 K strain and the PPS.

Appendix A. Supplementary data

Supplementary data associated with this article can be found, in the online version, at doi:10.1016/j.neulet.2011.04.072.

References

[1] R. Atarashi, K. Satoh, K. Sano, T. Fuse, N. Yamaguchi, D. Ishibashi, T. Matsubara, T. Nakagaki, H. Yamanaka, S. Shirabe, M. Yamada, H. Mizusawa, T. Kitamoto, G. Klug, A. McGlade, S.J. Collins, N. Nishida, Ultrasensitive human prion detection in cerebrospinal fluid by real-time quaking-induced conversion, Nat. Med. 17 (2011) 175–178.
[2] M.E. Bruce, R.G. Will, J.W. Ironside, I. McConnell, D. Drummond, A. Suttie, L. McCardle, A. Chree, J. Hope, C. Birkett, S. Cousens, H. Fraser, C.J. Bostock, Transmissions to mice indicate that 'new variant' CJD is caused by the BSE agent, Nature 389 (1997) 498–501.
[3] J. Castilla, P. Saá, C. Hetz, C. Soto, In vitro generation of infectious scrapie prions, Cell 121 (2005) 195–206.
[4] J. Castilla, P. Saá, R. Morales, K. Abid, K. Maundrell, C. Soto, Protein misfolding cyclic amplification for diagnosis and prion propagation studies, Methods Enzymol. 412 (2006) 3–21.
[5] J. Collinge, K.C. Sidle, J. Meads, J. Ironside, A.F. Hill, Molecular analysis of prion strain variation and the aetiology of 'new variant' CJD, Nature 383 (1996) 685–690.
[6] N.R. Deleault, R. Kascsak, J.C. Geoghegan, S. Supattapone, Species-dependent differences in cofactor utilization for formation of the protease-resistant prion protein in vitro, Biochemistry 49 (2010) 3928–3934.
[7] K. Doh-ura, K. Ishikawa, I. Murakami-Kubo, K. Sasaki, S. Mohri, R. Race, T. Iwaki, Treatment of transmissible spongiform encephalopathy by intraventricular drug infusion in animal models, J. Virol. 78 (2004) 4999–5006.
[8] J.A. Edgeworth, M. Farmer, A. Sicilia, P. Tavares, J. Beck, T. Campbell, J. Lowe, S. Mead, P. Rudge, J. Collinge, G.S. Jackson, Detection of prion infection in variant Creutzfeldt–Jakob disease: a blood-based assay, Lancet 377 (2011) 487–493.
[9] R. Gabizon, Z. Meiner, M. Halimi, S.A. Ben-Sasson, Heparin-like molecules bind differentially to prion-proteins and change their intracellular metabolic fate, J. Cell. Physiol. 157 (1993) 319–325.
[10] A.F. Hill, M. Desbruslais, S. Joiner, K.C. Sidle, I. Gowland, J. Collinge, L.J. Doey, P. Lantos, The same prion strain causes vCJD and BSE, Nature 389 (1997) 448–450, 526.
[11] M. Hizume, A. Kobayashi, K. Teruya, H. Ohashi, J.W. Ironside, S. Mohri, T. Kitamoto, Human prion protein (PrP) 219 K is converted to PrPSc but shows heterozygous inhibition in variant Creutzfeldt–Jakob disease infection, J. Biol. Chem. 284 (2009) 3603–3609.
[12] S. Ikeda, A. Kobayashi, T. Kitamoto, Thr but Asn of the N-glycosylation sites of PrP is indispensable for its misfolding, Biochem. Biophys. Res. Commun. 369 (2008) 1195–1198.
[13] J.W. Ironside, Variant Creutzfeldt–Jakob disease: risk of transmission by blood transfusion and blood therapies, Haemophilia 12 (Suppl. 1) (2006) 8–15, discussion 26-8.
[14] M. Jones, A.H. Peden, C.V. Prowse, A. Groner, J.C. Manson, M.L. Turner, J.W. Ironside, I.R. MacGregor, M.W. Head, In vitro amplification and detection of variant Creutzfeldt–Jakob disease PrPSc, J. Pathol. 213 (2007) 21–26.
[15] A. Kobayashi, M. Asano, S. Mohri, T. Kitamoto, Cross-sequence transmission of sporadic Creutzfeldt–Jakob disease creates a new prion strain, J. Biol. Chem. 282 (2007) 30022–30028.
[16] Y. Murayama, M. Yoshioka, K. Masujin, H. Okada, Y. Iwamaru, M. Imamura, Y. Matsuura, S. Fukuda, S. Onoe, T. Yokoyama, S. Mohri, Sulfated dextrans enhance in vitro amplification of bovine spongiform encephalopathy PrP(Sc) and enable ultrasensitive detection of bovine PrP(Sc), PLoS One 5 (2010) e13152.
[17] P. Parchi, A. Giese, S. Capellari, P. Brown, W. Schulz-Schaeffer, O. Windl, I. Zerr, H. Budka, N. Kopp, P. Piccardo, S. Poser, A. Rojiani, N. Streichemberger, J. Julien, C. Vital, B. Ghetti, P. Gambetti, H. Kretzschmar, Classification of sporadic Creutzfeldt–Jakob disease based on molecular and phenotypic analysis of 300 subjects, Ann. Neurol. 46 (1999) 224–233.
[18] P. Saá, J. Castilla, C. Soto, Ultra-efficient replication of infectious prions by automated protein misfolding cyclic amplification, J. Biol. Chem. 281 (2006) 35245–35252.
[19] G.P. Saborio, B. Permanne, C. Soto, Sensitive detection of pathological prion protein by cyclic amplification of protein misfolding, Nature 411 (2001) 810–813.
[20] C. Soto, L. Anderes, S. Suardi, F. Cardone, J. Castilla, M.J. Frossard, S. Peano, P. Saa, L. Limido, M. Carbonatto, J. Ironside, J.M. Torres, M. Pocchiari, F. Tagliavini, Presymptomatic detection of prions by cyclic amplification of protein misfolding, FEBS Lett. 579 (2005) 638–642.
[21] L. Thorne, L.A. Terry, In vitro amplification of PrPSc derived from the brain and blood of sheep infected with scrapie, J. Gen. Virol. 89 (2008) 3177–3184.
[22] C. Wong, L.W. Xiong, M. Horiuchi, L. Raymond, K. Wehrly, B. Chesebro, B. Caughey, Sulfated glycans and elevated temperature stimulate PrP(Sc)-dependent cell-free formation of protease-resistant prion protein, EMBO J. 20 (2001) 377–386.

Vaccine 29 (2011) 9321–9328

Contents lists available at SciVerse ScienceDirect

Vaccine

journal homepage: www.elsevier.com/locate/vaccine

Antigenic mimicry-mediated anti-prion effects induced by bacterial enzyme succinylarginine dihydrolase in mice

Daisuke Ishibashi[a], Hitoki Yamanaka[a], Tsuyoshi Mori[b], Naohiro Yamaguchi[a], Yoshitaka Yamaguchi[b], Noriyuki Nishida[a], Suehiro Sakaguchi[b,*]

[a] Department of Molecular Microbiology and Immunology, Nagasaki University Graduate School of Biomedical Sciences, 1-12-4 Sakamoto, Nagasaki 852-8523, Japan
[b] Division of Molecular Neurobiology, The Institute for Enzyme Research, The University of Tokushima, 3-18-15 Kuramoto-cho, Tokushima 770-8503, Japan

ARTICLE INFO

Article history:
Received 15 April 2011
Received in revised form
27 September 2011
Accepted 5 October 2011
Available online 18 October 2011

Keywords:
Prion
Vaccine
Antigenic mimicry
Humoral immunity

ABSTRACT

Prions, the causative agents of prion diseases, are immunologically tolerated because their major component, prion protein (PrP), is a host-encoded molecule. Therefore, no effective prion vaccines have been developed. We previously showed that heterologous bovine and sheep PrP immunizations of mice overcame tolerance by an antigenic mimicry mechanism to efficiently induce anti-PrP auto-antibodies (Abs), significantly prolonging incubation times in mice subsequently infected with the mouse-adapted Fukuoka-1 prion. These results prompted us to investigate if non-mammal derived molecules able to antigenically mimic anti-prion epitopes, could act as prion vaccines. We show here that immunization of mice with recombinant succinylarginine dihydrolase, a bacterial enzyme with a peptide sequence similar to an anti-prion epitope, induced anti-PrP auto-Abs with anti-prion activity and significantly retarded survival times of the mice subsequently infected with Fukuoka-1 prions. These results might open a way for development of a new type of antigenic mimicry-based prion vaccine.

1. Introduction

Prion diseases, which include Creutzfeldt–Jakob disease (CJD) in humans and bovine spongiform encephalopathy (BSE) and scrapie in animals, are neurodegenerative disorders caused by prions [1,2]. It is believed that BSE prions have been orally transmitted to humans via contaminated foods, causing a new variant type of CJD (vCJD) [3,4]. Fortunately, BSE incidence has been dramatically decreased, mainly due to the ban on using meat and bone meal ingredients in animal feed, thereby reducing the risk of BSE transmission to humans. In contrast, 4 vCJD cases were reported among recipients transfused with blood from donors who eventually developed vCJD [5–7], suggesting an increasing risk of secondary transmission of vCJD among human populations via medical treatments and/or procedures. However, no prophylactic vaccines against prion diseases have been developed.

Prions are mainly composed of the proteinase K (PK)-resistant prion protein, designated PrP^{Sc}, which is produced by conformational conversion of the normal cellular isoform, PrP^{C}, a glycosylphosphatidylinositol-anchored membrane glycoprotein abundantly expressed in neurons [1,2]. Thus, PrP is a potential candidate molecule for prion vaccines. Indeed, mice transgenically expressing 6H4 anti-PrP monoclonal antibody (mAb) developed the disease with very prolonged onset after intraperitoneal infection with mouse-adapted scrapie RML prions [8]. Moreover, passive immunization with anti-PrP mAbs, ICSM 18 and 35, markedly attenuated the disease in mice intraperitoneally infected with RML prions [9]. However, PrP is a host-encoded protein. Therefore, PrP vaccines might cause autoimmune reactions in an immunized host. In addition, PrP vaccines have another possible adverse effect as immunized PrPs might be converted into infectious PrPs or prions. Indeed, it was recently reported that recombinant mouse PrP (rMoPrP) mixed with RNAs and lipids, both of which are ubiquitous molecules *in vivo*, was converted into infectious PrP or a prion *in vitro* after being subjected to protein misfolding cyclic amplification (PMCA) [10]. These indicate that, molecules other than PrP, may be useful as prion vaccines.

We previously demonstrated that heterologous PrPs function as antigen mimicking molecules to host PrP [11]. Heterologous recombinant bovine and sheep PrPs were highly immunogenic in mice, efficiently inducing anti-PrP auto-Abs, and immunization with these proteins significantly prolonged incubation times in mice inoculated with the mouse-adapted Fukuoka-1 prion [11]. This therefore suggested that certain molecules, if able to antigenically mimic anti-prion epitopes, could behave as prion vaccines.

The aim of this study is to investigate this possibility. We show here that immunization of mice with recombinant succinylarginine dihydrolase (SADH), a bacterial molecule with a sequence similar

* Corresponding author. Tel.: +81 88 633 7438; fax: +81 88 633 7440.
E-mail address: sakaguch@ier.tokushima-u.ac.jp (S. Sakaguchi).

0264-410X/$ – see front matter © 2011 Elsevier Ltd. All rights reserved.
doi:10.1016/j.vaccine.2011.10.017

to the 6H4 anti-prion epitope, elicited Abs not only to itself but also crossreactive Abs to the 6H4 epitope of PrP. We also show that the anti-SADH sera possessed anti-prion activity, reducing PrP^{Sc} levels in prion-infected cells, and that immunization of the recombinant protein significantly retarded survival times of mice infected with Fukuoka-1 prions. These results suggest that antigenic mimicry-based prion vaccines might be considered as a new type of prion vaccine to be studied.

2. Materials and methods

2.1. Animals

4-Week old female BALB/c mice were purchased from SLC Japan, Shizuoka, Japan. Mice were cared for in accordance with the Guidelines for Animal Experimentation of Nagasaki University.

2.2. Expression and purification of recombinant proteins

A DNA fragment corresponding to residues 297–447 of SADH (GenBank accession no. U00096) of DH5α*Escherichia coli* was amplified by polymerase chain reaction (PCR) using a sense primer (3′-cc*ggatcc*gtatggggttatctcaatga-5′; italicized sequence, *Bam*HI site) and an anti-sense primer (3′-*gggtcgac*tccattgccccctccctcgcg-5′; italicized sequence, *Sal*I site). A DNA fragment encoding residues 331–447 of SADH of *Salmonella enterica* subspecies *enterica* serovar Paratyphi A str. ATCC 9150 (GenBank accession no. NC_006511) was also amplified by PCR using a sense primer (3′-c*ggatcc*tcagatgctgtggcgcccta-5′; italicized sequence, *Bam*HI site) and an anti-sense primer (3′-*gggtcgac*tccatcagccgccccgtttgct-5′; italicized sequence, *Sal*I site). Following sequence confirmation of the PCR products, the fragments were digested with *Bam*HI and *Sal*I and inserted into a pQE30 vector (QIAGEN, Hilden, Germany) and the vector developed to produce the protein of interest with an N-terminal 6× His tag. *E.coli*(M15) cells were freshly transformed by the plasmids, cultured in LB medium containing 1 mM isopropylthio-β-D-galactoside (IPTG), and collected by centrifugation. The collected cells were lysed using CelLytic B Bacterial Cell Lysis/Extraction Reagent (Sigma–Aldrich Co., St Louis, USA) in the presence of deoxyribonuclease I and the lysate was centrifuged at 25,000 × *g* for 10 min. The resulting pellet containing SADH protein was suspended in Reagent containing 0.2 mg/ml lysozyme and incubated with occasional shaking at room temperature (RT) for 15 min. Volume of the suspension was then increased by addition of 1:10 diluted Reagent and centrifuged at 25,000 × *g* for 10 min. The resulting pellet was washed 3 times with 1:10 diluted Reagent, suspended in lysis buffer (8 M Urea, 10 mM Tris–HCl, 100 mM Na_2HPO_4, pH 8.0) and SADH recombinant proteins were purified using a Ni-NTA column in denaturing conditions as recommended in the manufacturer's protocol.

Recombinant mouse PrP (rMoPrP) without a 6× His tag was expressed and purified as described elsewhere [11]. In brief, a DNA fragment corresponding to MoPrP 23–231 was amplified by PCR. Following sequence confirmation, this fragment was digested with *Nde*I and *Bam*HI and inserted into a pET11a vector (Novagen, Inc., WI, USA). *E. coli* (BL21) cells were transformed and cultured in LB medium. rMoPrP was purified by subjecting the extract of the cells into a CM-sepharose column (Amersham Pharmacia Biotech AB, Uppsala, Sweden).

2.3. Immunization

Purified recombinant proteins were dialyzed against PBS. 100 μg of the dialyzed protein was intraperitoneally inoculated into a 4-week-old female BALB/c mouse (SLC Japan) together with complete Freund's adjuvant (CFA; Difco Laboratories, Detroit, MI) for the first immunization. Additional immunizations were performed by intraperitoneal inoculation of the same amounts of the protein with incomplete Freund's adjuvant (Difco Laboratories) into the mice at 2-week intervals. Antisera were collected one week after the final immunization and stored at −20 °C until used.

2.4. Enzyme-linked immunosorbent assay (ELISA)

For detection of purified SADH recombinant proteins or rMoPrP without a 6× His tag, each well of a 96 well immunoplate (Nunc, Roskilde, Denmark) was coated with 500 ng of the proteins by overnight incubation at 4 °C and then blocked with PBS containing 0.05% Tween-20 (T-PBS) and 25% Blocking One (Nakarai tesque Co., Kyoto, Japan) at 37 °C for 1 h. To detect specific IgG Abs, serially 10-fold diluted antiserum was added to the wells for 1 h at 37 °C and unbound Abs were removed by washing twice with T-PBS. Immune complexes were detected using secondary goat anti-mouse IgG Abs conjugated with HRP (GE Healthcare, Buckinghamshire, England), 2 mM 2,2′-azino-bis(3-ethylbenzthiazoline-6-sulfonic acid), and 0.04% H_2O_2. Antibody titers were determined using colorimetric values expressed at 405 nm.

For detection of a MoPrP peptide 131–154 (>70% purity, Sigma–Aldrich Japan K.K., Hokkaido, Japan), we used a more sensitive ELISA system. 1 μg of the peptide was coated on a 96 well immunoplate (Nunc) and similarly subjected to the procedures described above except that the immunocomplexes were detected using 3,3′,5,5′-tetramethylbenzidine (Pierce, Rockford, IL) at 450 nm.

2.5. Fluorescence-activated cell sorter (FACS) analysis

PrP^C-deficient hippocampal neurons, designated HpL3-4 [12], and HpL3-4 cells overexpressing exogenous PrP^C, designated HpL3-4TR [12] (provided by Prof. Onodera, The University of Tokyo, Japan), were harvested in PBS containing 20 mM EDTA. Cells were then suspended in BSS buffer (140 mM NaCl, 5.4 mM KCl, 0.8 mM $MgSO_4$, 0.3 mM Na_2HPO_4, 0.4 mM KH_2PO_4, and 1 mM $CaCl_2$) containing 5% fetal bovine serum (FBS), and incubated with 100-fold diluted antisera for 1 h on ice. The treated cells were then washed 3 times with BSS buffer containing 5% FBS, reacted with Alexa Fluor® 546 goat anti-mouse IgG (Invitrogen, Carlsbad, CA) and analyzed using a flow cytometer (BD FACSCanto™ II Flow Cytometer, BD Biosciences, San Jose, CA).

2.6. Western blotting analysis

Total proteins of cell lysates treated with or without 20 μg/ml of proteinase K (PK) (Sigma–Aldrich Co.) at 37 °C for 30 min were separated on 15% SDS-PAGE and electrically transferred onto a PVDF membrane (Millipore, MA, USA). The PK activity was blocked by boiling in a buffer (50 mM Tris–HCl, pH 6.8, 5% glycerol, 1.6% SDS, 100 mM dithiothreitol) for 5 min. The membrane was immersed in TBST (0.1% Tween 20, 100 mM NaCl, 10 mM Tris–HCl, pH 7.6) containing 5% nonfat dry milk and then incubated either with 1:5000-diluted M-20 anti-PrP goat polyclonal Ab (Santa Cruz Biotechnology, Inc., Santa Cruz, CA) to detect PrP or with 1:5000-diluted Ab against β-actin (Sigma–Aldrich Co.). Immune complexes were visualized using secondary sheep anti-mouse IgG Abs conjugated with HRP (GE Healthcare) and the ECL system (GE Healthcare).

2.7. In vitro assay of anti-prion activity of anti-sera

The *in vitro* anti-prion activity of antisera was assessed by their activities to reduce PrP^{Sc} levels in mouse neuroblastoma N2a cell line persistently infected with a mouse-adapted Fukuoka-1 prion,

termed N2a58-Fk [13]. The cells were cultured in DMEM containing 10% FBS. 2×10^5 cells in one well of a 6 well plate were incubated with 1:10 or 1:50-diluted antisera for 2 days. The cells were then lysed in a lysis buffer (1% TritonX-100, 1% sodium deoxycholate, 300 mM NaCl, and 100 mM Tris–HCl, pH 7.5) and the lysates were subjected to Western blotting.

2.8. Prion inoculation

Brains were removed from diseased mice infected with the mouse-adapted Fukuoka-1 prion [14] and then homogenized to 1% (w/v) in PBS. Aliquots (100 μl) of the homogenate were intraperitoneally inoculated into each mouse 1 week after receiving 5 immunizations.

2.9. Cell viability assay

Cell viability was determined by usingthe PreMix WST-1 Cell Proliferation Assay System (Takara Bio Inc., Shiga, Japan). N2a58 cells were plated on 96-well plates at a density of 5×10^3 cells/well in 100 μl of Dulbecco's Modified Eagle Medium (DMEM) containing 10% FBS. On the next day, each of the antisera was added into the culture medium at the final concentration of 10%. After 48 h, the WST-1 assay was performed according to the manufacturer's instructions. In brief, the cells treated with antisera were incubated with PreMix WST-1 substances for 3 h at 37 °C, and then their absorbance was measured at 450 nm.

2.10. Histology

The brain tissues of mice were fixed in 4% paraformaldehyde and sectioned into 5-μm-thick sections after paraffin embedding. The tissue sections were stained with hematoxylin and eosin (HE).

2.11. Statistical analysis

Logrank test was used for analysis of the survival times of mice. Colorimetric data from ELISA were subjected to one way ANOVA followed by Tukey–Kramer multiple comparison testing.

3. Results

3.1. Bacterial enzyme SADH has an amino acid sequence similar to 6H4 anti-prion epitope

We selected the 6H4 anti-prion epitope, which corresponds to residues 144–152 of MoPrP [15] (Fig. 1A), as a target sequence because this epitope overlaps the ICSN18 anti-prion epitope (residues 146–159) [9], and both 6H4 and ICSN18 mAbs have already been demonstrated to be effective against prions in mice [8,9]. We then searched for non-mammal-derived molecules with sequences similar to the epitope using Basic Local Alignment Search Tool in the National Center for Biotechnology Information website (http://blast.ncbi.nlm.nih.gov/Blast.cgi). As a result, we found a 6H4-mimicking sequence in the bacterial enzyme SADH (Fig. 1A). SADH is a much conserved molecule involved in the arginine succinyltransferase pathway in *E. coli* and related bacteria including *S. enterica* subspecies, *Klebsiella aerogenes* and *Pseudomonas aeruginosa* [16].

3.2. SADHs elicit marked Ab responses in mice

To investigate whether or not SADH proteins could be immunogenic in mice, we first recombinantly expressed and purified the recombinant SADH protein from *E. coli* [hereafter referred to as SADH(*E*)] or *S. enterica* subspecies *enterica* serovar Paratyphi A strain [hereafter referred to as SADH(*S*)] (Fig. 1B). The recombinant proteins were designed to have the mimicking sequence at the center and a 6 × His sequence at the N-terminus. The SADH(*S*) recombinant protein was higher than SADH(*E*) in molecular weight because of an additional 35 amino acids in the N-terminal region. The purified recombinant proteins were then intraperitoneally inoculated into BALB/c mice 5 times at 2-week intervals. We collected antisera from the mice 1 week after the final immunization and subjected them to an ELISA to detect specific IgG responses against the respective immunogens. No increase in optical density values at 405 nm (OD_{405}) was observed against SADH(*E*) and SADH(*S*) immunogens with control sera from non-immunized mice (Fig. 1C). In contrast, anti-SADH(*E*) and anti-SADH(*S*) sera from each of the immunized mice showed very high OD_{405} values against the respective immunogens (Fig. 1C). These results indicate that SADH(*E*) and SADH(*S*) recombinant proteins are highly immunogenic in mice, inducing very high Ab responses.

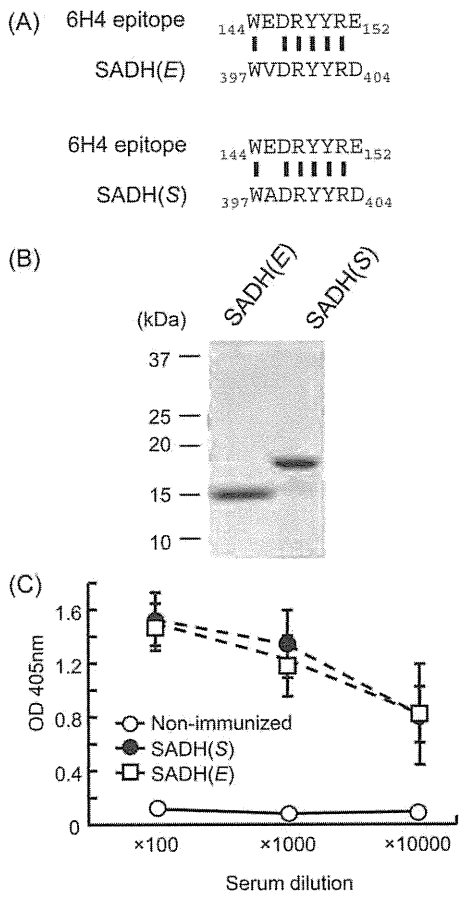

Fig. 1. High immunogenicity of the bacterial enzyme SADHs carrying a sequence mimicking the 6H4 anti-prion epitope in mice. (A) Comparison of the amino acid sequence of the 6H4 anti-prion epitope to the mimic sequences of SADH(*E*) and SADH(*S*). Arabic numbers represent the codon number of each indicated amino acid in each molecule. (B) Coomassie brilliant blue staining of purified SADH(*E*) and SADH(*S*) recombinant proteins. (C) The OD_{405} values of anti-SADH(*E*) and anti-SADH(*S*) sera against the respective antigens evaluated by an ELISA. Purified recombinant protein was intraperitoneally inoculated into BALB/c mice 5 times at 2-week intervals and anti-sera were taken 1 week after the final immunization. Compared to control sera from non-immunized mice ($n = 6$), anti-SADH(*E*) ($n = 21$) and anti-SADH(*S*) sera ($n = 20$) showed very high OD_{405} values against the respective immunogens.

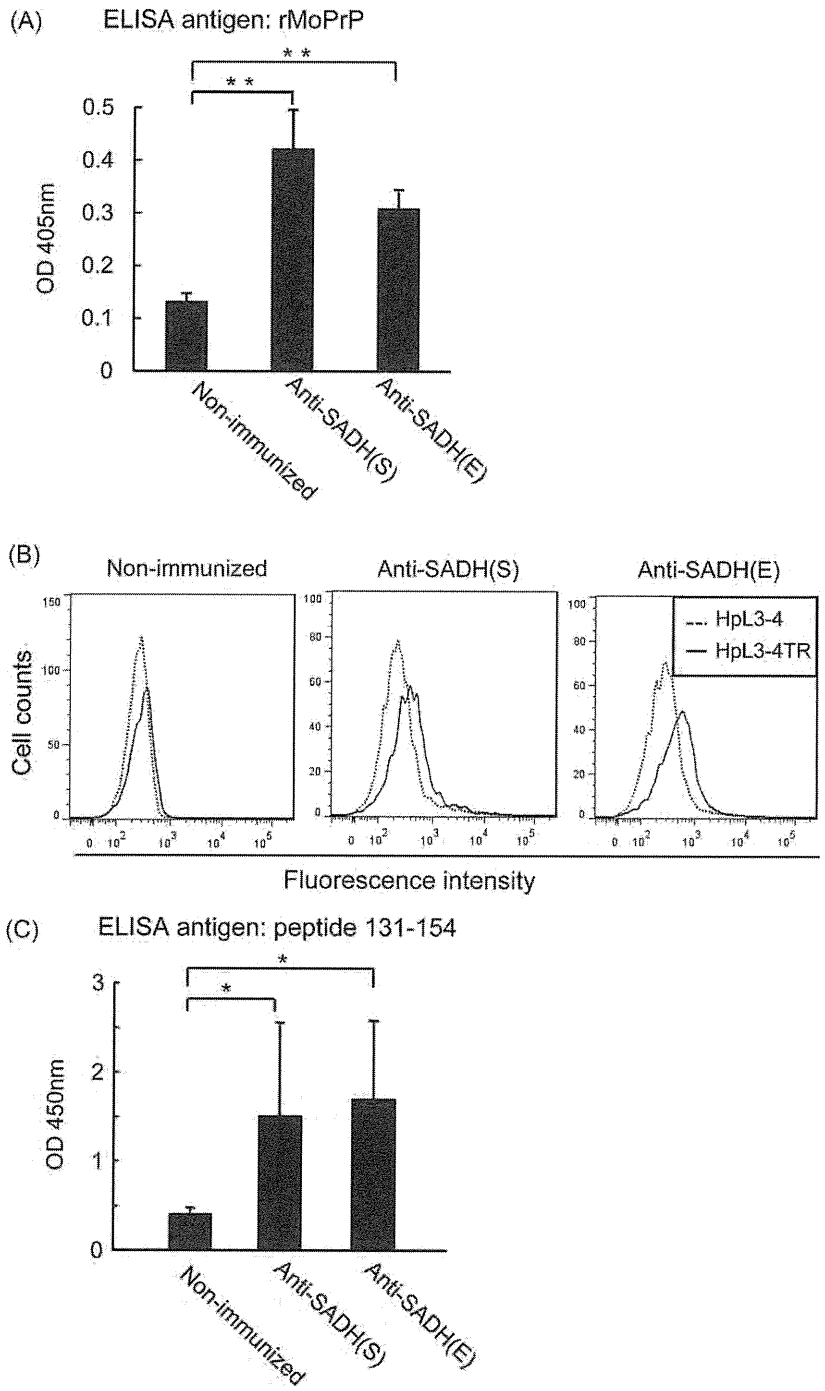

Fig. 2. SADH recombinant proteins induce anti-PrP auto-Abs able to recognize the 6H4 anti-prion epitope. (A) Anti-SADH(*E*) and anti-SADH(*S*) sera recognize full-length rMoPrP. Anti-SADH(*E*) ($n=10$) and anti-SADH(*S*) sera ($n=9$) were diluted 1:20 and subjected to an ELISA against purified rMoPrP without a 6× His tag. Higher OD_{405} values were detected with anti-SADH(*E*) and anti-SADH(*S*) sera than those of control sera ($n=9$) from non-immunized mice. (B) Anti-SADH(*E*) and anti-SADH(*S*) sera recognize PrP^C on the cell surface. HpL3-4 and HpL3-4TR cells were subjected to FACS analysis with the antisera. PrP^C on the HpL3-4TR cells was detected by the anti-SADH(*E*) (middle panel) and anti-SADH(*S*) sera (right panel) but not by non-immunized sera (left panel). (C) Anti-SADH(*E*) ($n=16$) and anti-SADH(*S*) sera ($n=15$) recognize the 6H4 anti-prion epitope. To investigate anti-SADH(*E*) and anti-SADH(*S*) sera for their binding activity to a 6H4 epitope-containing PrP peptide, we employed a more sensitive ELISA as described in Section 2. Anti-SADH(*E*) and anti-SADH(*S*) sera were diluted at 1:20 and subjected to the ELISA using the PrP peptide 131–154 encompassing the 6H4 epitope as an antigen. This sensitive ELISA resulted in higher backgrounds. However, significantly higher OD_{450} values were detected with anti-SADH(*E*) and anti-SADH(*S*) sera, compared to those with control non-immunized sera ($n=6$). $^*p<0.05$; $^{**}p<0.01$.

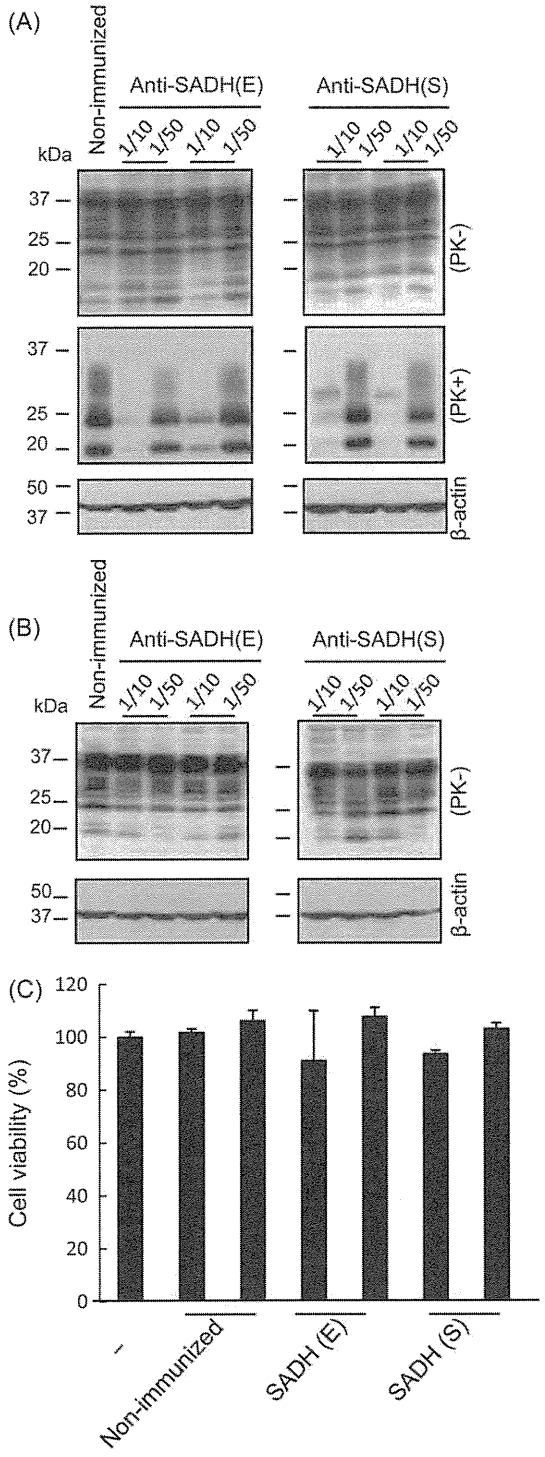

Fig. 3. *In vitro* anti-prion activity of anti-SADH(*E*) and anti-SADH(*S*) sera. (A) Anti-SADH(*E*) and anti-SADH(*S*) sera reduce PrP^{Sc} levels in prion-infected cells. N2a58-Fk cells were incubated for 2 days with anti-SADH(*E*) ($n=2$) and anti-SADH(*S*) sera ($n=2$) at indicated dilutions and then subjected to Western blotting. Compared to non-immunized sera, anti-SADH(*E*) or anti-SADH(*S*) sera reduced PrP^{Sc} levels in the cells in a dose-dependent manner without affecting the level of total PrP. (B) Anti-SADH(*E*) and anti-SADH(*S*) sera do not reduce PrP^{C} levels in uninfected cells. N2a58 cells were similarly incubated with anti-SADH(*E*) ($n=2$) and anti-SADH(*S*) sera ($n=2$). No significant reduction in the PrP^{C} level was detected in these cells. (C) Anti-SADH(*E*) and anti-SADH(*S*) sera are not cytotoxic. N2a58 cells were similarly incubated without (–) or with non-immunized ($n=2$), anti-SADH(*E*) ($n=2$) and anti-SADH(*S*) sera ($n=2$) and then subjected to a cell viability assay. No significant reduction in the cell viability was detected in these cells.

3.3. SADHs induce anti-PrP auto-Abs in mice

We then investigated whether or not SADH proteins could induce anti-PrP auto-Abs in mice. Since the immunizing recombinant proteins contained a 6× His tag, we used untagged rMoPrP as an ELISA antigen to eliminate reactivity against the tag with crossreacting Abs that might be produced in the immunized mice. Compared to non-immunized sera, significantly higher OD_{405} values were detected with anti-SADH(*E*) and anti-SADH(*S*) sera (Fig. 2A). These results indicate that immunization with SADHs could induce anti-PrP auto-Abs in mice. We also investigated whether the antisera could recognize native PrP or PrP^{C} expressed on the cell surface using FACS analysis. HpL3-4 cells are devoid of PrP^{C} while HpL3-4TR cells express abundant PrP^{C} on their surface. Non-immunized sera induced no signal shift of HpL3-4TR cells, compared to the signal of HpL3-4 cells (Fig. 2B, left panel). In contrast, the signal of HpL3-4TR cells was slightly but distinctly shifted to the right by the anti-SADH(*S*) (Fig. 2B, middle panel) and anti-SADH(*E*) sera (Fig. 2B, right panel), indicating that the anti-SADH sera recognize PrP^{C} expressed on the cell surface.

3.4. Anti-SADH sera recognize the 6H4 anti-prion epitope

SADH(*E*) and SADH(*S*) recombinant proteins have an amino acid sequence similar to the 6H4 anti-prion epitope. We therefore investigated if anti-SADH(*E*) and anti-SADH(*S*) sera could react with the epitope using an ELISA with a PrP peptide 131–154, which encompasses the 6H4 epitope. We used a more sensitive ELISA for detecting the peptide because the conventional ELISA used for detection of full-length rMoPrP was less sensitive to detecting the specific signals of the peptide [11]. This sensitive ELISA resulted in higher backgrounds from non-immunized sera (Fig. 2C). However, the 20-fold diluted anti-SADH(*E*) and anti-SADH(*S*) sera showed significantly higher OD_{450} values, compared to control non-immunized sera (Fig. 2C), indicating that SADH(*E*) and SADH(*S*) recombinant proteins induce anti-PrP auto-Abs reacting with the 6H4 anti-prion epitope in mice.

3.5. Anti-SADH sera decrease PrP^{Sc} levels in a prion-infected cell line

We also investigated if anti-SADH sera could have anti-prion activities. Mouse neuroblastoma N2a cell line persistently infected with Fukuoka-1 prions, termed N2a58-Fk, was incubated for 2 days with 10 or 50-fold diluted anti-sera and thereafter subjected to Western blotting with M-20 anti-PrP Ab, which recognizes the C-terminal part of PrP. Anti-SADH(*E*) or anti-SADH(*S*) sera taken from two immunized mice reduced PrP^{Sc} levels in the cells in a dose-dependent manner, compared to the PrP^{Sc} levels in the cells treated with non-immunized sera (Fig. 3A). Total PrP levels in N2a58-Fk and PrP^{C} levels in uninfected parental N2a58 cells were not affected by the treatment with these antisera (Fig. 3A and B). No cytotoxicity was detected with these antisera in N2a58 cells (Fig. 3C). These results indicate that immunization with SADH(*E*) and SADH(*S*) recombinant proteins induce anti-prion Abs in mice, and that anti-SADH(*E*) or anti-SADH(*S*) sera are effective against prions in N2a58-Fk cells without affecting the PrP^{C} levels.

Table 1
Prophylactic effects of immunization with SADHs on prion infection.

Immunogen	Survival times (Mean ± SD, days)	No. of mice (diseased/total)	*p*-Values (Logrank test)
–	298 ± 28	10/10	
SADH(*E*)	329 ± 15	5/5	0.0284
SADH(*S*)	321 ± 15	5/5	0.0384

3.6. Effects of immunization with SADH recombinant proteins against mouse-adapted prion in mice

We investigated the effects of the immunization with SADH recombinant proteins against prions. BALB/c mice were intraperitoneally immunized with purified recombinant SADH(*E*) and SADH(*S*) proteins 5 times at 2-week intervals and thereafter intraperitoneally inoculated with Fukuoka-1 prion 1 week after the final immunization. Non-immunized mice eventually died of the disease 298 ± 28 days post-inoculation (p.i.) (Table 1). However, mice immunized with SADH(*E*) and SADH(*S*) recombinant proteins displayed significantly longer survival times at 329 ± 15 ($p = 0.0284$) and 321 ± 21 days p.i. ($p = 0.0384$), respectively (Table 1). HE staining of the brains of terminally ill mice either immunized with the recombinant proteins or non-immunized revealed indistinguishably abundant vacuoles throughout the brains, particularly in the cortex, the thalamus and the cerebellar white matter (Fig. 4). Hippocampal neurons seemed undamaged in the immunized mice, compared to those in non-immunized control mice (Fig. 4). No lymphocyte infiltration was detected in the brains of the immunized and non-immunized mice by immunohistochemistry using anti-T cell Abs, including anti-CD4 and anti-CD8 Abs, and an anti-B cell Ab, such as anti-CD45R Ab (data not shown). These results indicate that immunization with SADH(*E*) and SADH(*S*) recombinant proteins are effective against prion infection in mice without affecting the final pathology in the brain.

4. Discussion

In the present study, we showed that the bacterial enzymes SADH(*E*) and SADH(*S*), which carry a peptide sequence mimicking the 6H4 anti-prion epitope, are highly immunogenic in mice, eliciting Ab responses against not only themselves but also the

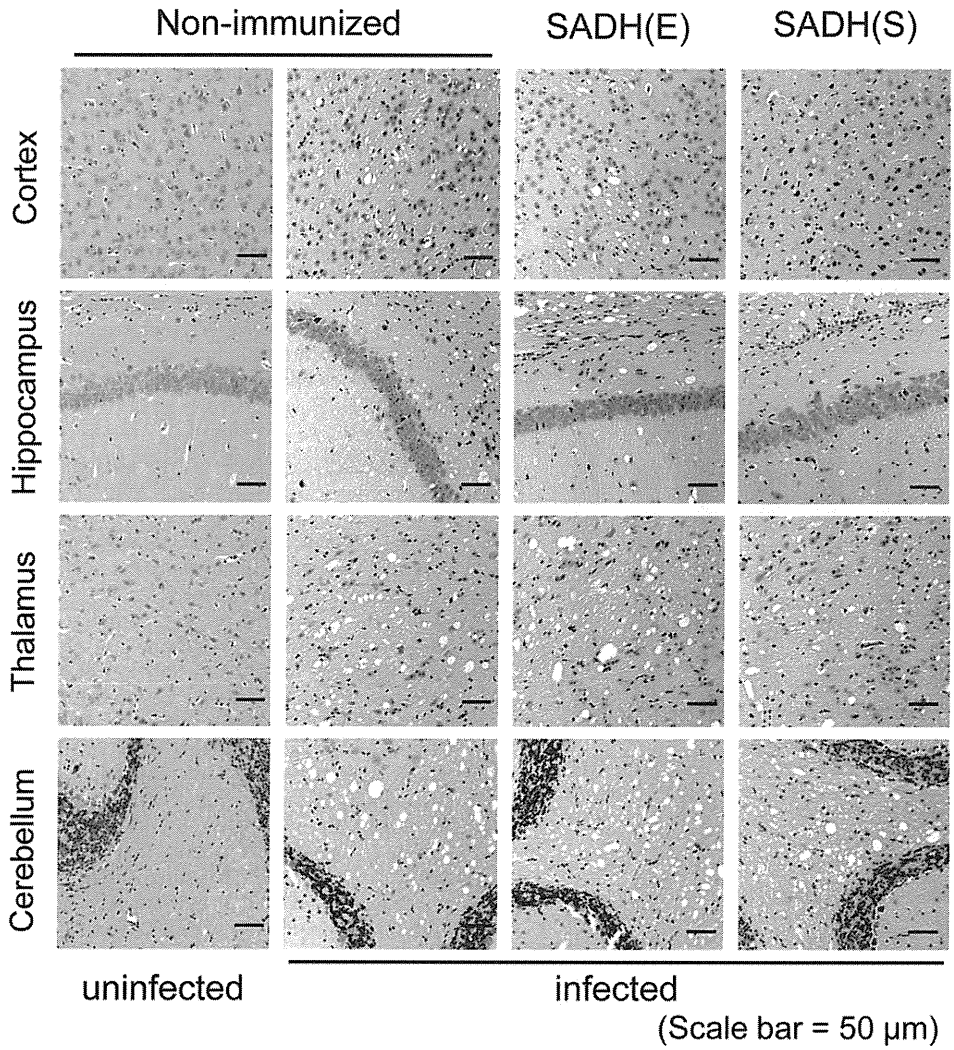

Fig. 4. HE staining of the brains of terminally ill mice with or without SADH recombinant protein immunization. No disease-specific vacuoles were observed in the brains of uninfected mice. In contrast, terminally ill mice either immunized with the recombinant proteins or not, exhibited many vacuoles indistinguishably over their brains.

6H4 epitope. We also showed that anti-SADH(*E*) and anti-SADH(*S*) sera were able to prevent PrP^{Sc} formation in N2a cells that were persistently infected with Fukuoka-1 prion, and that immunization with the recombinant proteins significantly prolonged survival times in mice subsequently infected with Fukuoka-1 prion. These results indicate that the 6H4 mimicking sequence in SADH(*E*) and SADH(*S*) recombinant proteins was immunogenic in mice, eliciting anti-prion Abs that recognize the 6H4 epitope and thereby exerting anti-prion activities.

We previously showed that immunization of CFA with rMoPrP into BALB/c mice with the same regimen as we employed in this study had no effects on the survival times of the mice intraperitoneally infected with Fukuoka-1 prion [11]. In contrast, the same immunization using CFA with heterologous bovine or sheep rPrP significantly extended the survival times of the immunized mice [11]. rMoPrP was immunologically tolerated in BALB/c mice while bovine and sheep rPrPs were highly immunogenic in BALB/c mice, inducing anti-PrP auto-Abs [11]. These results clearly indicate that the anti-prion effects in BALB/c mice immunized with SADH(*E*) and SADH(*S*) recombinant proteins are due to the immunization of the recombinant proteins, not due to the CFA.

The exact mechanism for the protective effects of the immunization with SADH(*E*) and SADH(*S*) recombinant proteins against the prion infection remains unknown. The peripherally inoculated prions first accumulate in the peripheral lymphoreticular tissues, such as spleen and lymph nodes, before invading the central nervous system. White et al. showed that passive immunization of anti-PrP mAbs, ICSM 18 and 35, into the peritoneal cavity markedly reduced accumulation of PrP^{Sc} and infectivity in the spleen of mice intraperitoneally infected with RML prions and attenuated the disease in these mice [9]. However, the same administration of these mAbs showed no effect on the disease in the mice already developing clinical symptoms or intracerebrally infected with the prions [9]. This is probably because Abs are unable to efficiently infiltrate the brain across the blood–brain barrier. These results indicate that substantial suppression of peripheral prion replication early in the incubation period could be protective against prion diseases. However, at present, we do not know whether immunization with SADH(*E*) and SADH(*S*) recombinant proteins would be effective against the peripheral prion replication.

Significantly higher OD_{450} values were obtained by ELISA with anti-SADH sera against peptide 131–154, which encompasses the 6H4 epitope, clearly indicating that the immunization with SADH(*E*) and SADH(*S*) recombinant proteins elicited Abs reactive with the 6H4 epitope in mice. Instead of the conventional ELISA used for detection of full-length rMoPrP, we used a more sensitive ELISA for detecting peptide 131–154. This is because we previously observed that the conventional ELISA was less sensitive for detecting the specific signals of the peptide with the antisera that were raised against heterologous bovine and sheep rPrPs in mice [11]. However, due to the different ELISA systems we used for detection of rMoPrP and the peptide, it remains unclear that the specific signals detected for full-length rMoPrP on the conventional ELISA would reflect those for the 6H4 epitope.

Most of the studies so far reported for prion vaccines utilized PrP molecules as vaccine antigens. Sigurdsson et al. showed that subcutaneous immunization of rMoPrP induced anti-PrP auto-Abs and slightly retarded onset of the disease by 16 days in mice subsequently infected with a mouse-adapted 139A prion [17]. However, other investigators reported that rMoPrP failed to induce anti-PrP auto-Abs in mice [18]. We also showed that neither anti-PrP auto-Abs nor prophylactic effects against Fukuoka-1 prions were observed in mice immunized with rMoPrP [11]. These results indicate that autologous PrP might not be necessarily immunogenic enough to overcome the tolerance. Modifications of PrP, including fusion with immunomodulatory proteins such as non-toxic fragment of heat-labile enterotoxin B subunit and heat shock proteins, were reported to enhance the immunogenicity of the fused PrP in mice [19,20]. In addition, we showed that heterologous PrPs are immunogenic enough to disrupt the tolerance by demonstrating that immunization with recombinant bovine and sheep PrPs efficiently elicited anti-PrP Abs in mice and significantly prolonged onset of the disease in the mice subsequently infected with Fukuoka-1 prions [11]. These results suggest that PrP molecules might be feasible candidates for prion vaccines.

PrP vaccines may risk causing adverse effects in the immunized host. First, it was shown that certain anti-PrP mAbs against residues 95–105 or the octapeptide repeat region were neurotoxic in mice, causing neuronal cell death [21,22]. Thus, PrP vaccines might induce such neurotoxic anti-PrP Abs in the immunized host. Second, since PrP is a host protein, PrP vaccines might cause autoimmune responses in the immunized host. Third, importantly, it was reported that rMoPrP was converted into infectious PrP *in vitro* by incubating with ubiquitous molecules, RNAs and lipids, and being subjected to PMCA [10]. Thus, PrP vaccines might have the possibility that immunizing PrP molecules are converted into infectious PrPs or prions in the immunized host. Considering these potential risks, PrP vaccines might be unfavorable as prion vaccines.

SADH(*E*) and SADH(*S*) contain a sequence mimicking the 6H4 epitope, but their overall amino acid sequences are quite different from PrPs. Therefore, unlike PrPs, SADH(*E*) and SADH(*S*) have no potential to be converted into an infectious molecule. No autoimmune responses were also reported in mice transgenically expressing 6H4 mAb [15]. PrP^{C} is most abundantly expressed in the brain. However, we detected no lymphocyte infiltration in the brains of terminally ill mice immunized with the recombinant proteins on immunohistochemical analysis. Moreover, no neurotoxic effects were shown with 6H4 mAb in mice [15]. Indeed, on inspection, we did not detect any abnormal behaviors in mice immunized with SADH(*E*) and SADH(*S*) recombinant proteins, compared to non-immunized mice. Hippocampal neurons were shown to be very vulnerable to the toxicity of 4H11 anti-PrP antibody in mice [21,22]. However, we observed no significant loss of hippocampal neurons in terminally ill mice immunized with SADH(*E*) and SADH(*S*) recombinant proteins. Taken together, these indicate that SADH(*E*) and SADH(*S*) recombinant proteins as antigens lack the adverse effects that might be potentially induced by PrP vaccines. Therefore, our present results suggest that, rather than PrP molecules, SADH(*E*) and SADH(*S*) or other non-mammal derived molecules carrying an amino acid sequence(s) antigenically mimicking the anti-prion epitopes could be candidate molecules for study as prion vaccines.

However, immunization with SADH(*E*) and SADH(*S*) recombinant proteins displayed significant but slight effects against Fukuoka-1 prions in mice. The increase in incubation times for the disease closely correlates with the titers of anti-PrP auto-Abs produced in immunized mice [17,23]. Sigurdsson et al. showed that mice producing higher titers of anti-PrP auto-Abs in plasma after subcutaneous immunization with mouse recombinant PrP developed the disease with longer incubation times after intraperitoneal infection with 139A prions. It was also reported that the protective effects of oral immunization with a mouse PrP-expressing attenuated *Salmonella typhimurium* LVR01 LPS vaccine strain against oral prion infection were nicely correlated to the titers of anti-PrP IgG and IgA auto-Abs produced in the immunized mice [23]. It is thus suggested that the modest effects of the immunization with SADH(*E*) and SADH(*S*) recombinant proteins against Fukuoka-1 prions might be attributable to low titers of the anti-PrP auto-Abs produced in the immunized mice. Indeed, anti-SADH(*E*) and anti-SADH(*S*) sera showed very low OD_{405} values against rMoPrP on the ELISA, compared to those against recombinant SADH(*E*) and SADH(*S*) proteins. Thus, further studies are required to enhance

the antigenicity of the mimic sequence in SADH(*E*) and SADH(*S*) recombinant protein to induce much higher titers of anti-prion Abs, enough to effectively prevent prion infection. Furthermore, it might be interesting to search for other non-mammalian molecules carrying an anti-prion epitope-mimic sequence(s) with higher antigenic properties. SADH is a very conserved molecule in *E. coli*, *S. enterica* subspecies, *K. aerogenes* and *P. aeruginosa* [16]. Therefore, it might be of interest to investigate whether or not individuals exposed to these pathogens might carry anti-prion Abs.

5. Conclusion

We show here that immunization with the bacterial molecules SADH(*E*) and SADH(*S*), which carry a sequence similar to the 6H4 anti-prion epitope, elicited anti-prion Abs in mice and significantly retarded survival times of the mice infected with Fukuoka-1 prions. This indicates that antigenic mimicry-based prion vaccines might be a new type of prion vaccine worth studying.

Acknowledgments

We thank Ryuichiro Atarashi, Katsuya Satoh, Takehiro Nakagaki, Takayuki Fuse, Takehiro Matsubara, Kazunori Sano, for helpful discussions, and Mari Kudo for technical assistance. This work was supported in part by the global COE Program (F12); a Grant-in-Aid for Young Scientists (B) (No. 22790955) from the Ministry of Education, Culture, Sports, Science, and Technology of Japan; a grant for BSE research, and a grant-in-aid of the Research Committee of Prion disease and Slow Virus Infection, from the Ministry of Health, Labor and Welfare of Japan.

References

[1] Prusiner SB. Prions. Proc Natl Acad Sci USA 1998;95(23):13363–83.
[2] Weissmann C, Enari M, Klohn PC, Rossi D, Flechsig E. Molecular biology of prions. Acta Neurobiol Exp (Warsz) 2002;62(3):153–66.
[3] Hill AF, Desbruslais M, Joiner S, Sidle KC, Gowland I, Collinge J, et al. The same prion strain causes vCJD and BSE. Nature 1997;389(6650):448–50.
[4] Bruce ME, Will RG, Ironside JW, McConnell I, Drummond D, Suttie A, et al. Transmissions to mice indicate that 'new variant' CJD is caused by the BSE agent. Nature 1997;389(6650):498–501.
[5] Llewelyn CA, Hewitt PE, Knight RS, Amar K, Cousens S, Mackenzie J, et al. Possible transmission of variant Creutzfeldt–Jakob disease by blood transfusion. Lancet 2004;363(9407):417–21.
[6] Peden AH, Head MW, Ritchie DL, Bell JE, Ironside JW. Preclinical vCJD after blood transfusion in a PRNP codon 129 heterozygous patient. Lancet 2004;364(9433):527–9.
[7] Zou S, Fang CT, Schonberger LB. Transfusion transmission of human prion diseases. Transfus Med Rev 2008;22(1):58–69.
[8] Heppner FL, Musahl C, Arrighi I, Klein MA, Rulicke T, Oesch B, et al. Prevention of scrapie pathogenesis by transgenic expression of anti-prion protein antibodies. Science 2001;294(5540):178–82.
[9] White AR, Enever P, Tayebi M, Mushens R, Linehan J, Brandner S, et al. Monoclonal antibodies inhibit prion replication and delay the development of prion disease. Nature 2003;422(6927):80–3.
[10] Wang F, Wang X, Yuan CG, Ma J. Generating a prion with bacterially expressed recombinant prion protein. Science 2010;327(5969):1132–5.
[11] Ishibashi D, Yamanaka H, Yamaguchi N, Yoshikawa D, Nakamura R, Okimura N, et al. Immunization with recombinant bovine but not mouse prion protein delays the onset of disease in mice inoculated with a mouse-adapted prion. Vaccine 2007;25(6):985–92.
[12] Kuwahara C, Takeuchi AM, Nishimura T, Haraguchi K, Kubosaki A, Matsumoto Y, et al. Prions prevent neuronal cell-line death. Nature 1999;400(6741):225–6.
[13] Nishida N, Katamine S, Manuelidis L. Reciprocal interference between specific CJD and scrapie agents in neural cell cultures. Science 2005;310(5747):493–6.
[14] Tateishi J, Ohta M, Koga M, Sato Y, Kuroiwa Y. Transmission of chronic spongiform encephalopathy with kuru plaques from humans to small rodents. Ann Neurol 1979;5(6):581–4.
[15] Korth C, Stierli B, Streit P, Moser M, Schaller O, Fischer R, et al. Prion (PrPSc)-specific epitope defined by a monoclonal antibody. Nature 1997;390(6655):74–7.
[16] Cunin R, Glansdorff N, Pierard A, Stalon V. Biosynthesis and metabolism of arginine in bacteria. Microbiol Rev 1986;50(3):314–52.
[17] Sigurdsson EM, Brown DR, Daniels M, Kascsak RJ, Kascsak R, Carp R, et al. Immunization delays the onset of prion disease in mice. Am J Pathol 2002;161(1):13–7.
[18] Polymenidou M, Heppner FL, Pellicioli EC, Urich E, Miele G, Braun N, et al. Humoral immune response to native eukaryotic prion protein correlates with anti-prion protection. Proc Natl Acad Sci USA 2004;101(Suppl. 2):14670–6.
[19] Yamanaka H, Ishibashi D, Yamaguchi N, Yoshikawa D, Nakamura R, Okimura N, et al. Enhanced mucosal immunogenicity of prion protein following fusion with B subunit of *Escherichia coli* heat-labile enterotoxin. Vaccine 2006;24(15):2815–23.
[20] Koller MF, Grau T, Christen P. Induction of antibodies against murine full-length prion protein in wild-type mice. J Neuroimmunol 2002;132(1–2):113–6.
[21] Solforosi L, Criado JR, McGavern DB, Wirz S, Sanchez-Alavez M, Sugama S, et al. Cross-linking cellular prion protein triggers neuronal apoptosis in vivo. Science 2004;303(5663):1514–6.
[22] Lefebvre-Roque M, Kremmer E, Gilch S, Zou WQ, Feraudet C, Gilles CM, et al. Toxic effects of intracerebral PrP antibody administration during the course of BSE infection in mice. Prion 2007;1(3):198–206.
[23] Goni F, Prelli F, Schreiber F, Scholtzova H, Chung E, Kascsak R, et al. High titers of mucosal and systemic anti-PrP antibodies abrogate oral prion infection in mucosal-vaccinated mice. Neuroscience 2008;153(3):679–86.

doi:10.1016/j.jmb.2011.08.043 J. Mol. Biol. (2011) 413, 667–683

Contents lists available at www.sciencedirect.com

Journal of Molecular Biology

journal homepage: http://ees.elsevier.com.jmb

Binding and Selectivity of the Marine Toxin Neodysiherbaine A and Its Synthetic Analogues to GluK1 and GluK2 Kainate Receptors

Masaki Unno[1,2,3*], Masanobu Shinohara[2], Koichiro Takayama[2], Hideharu Tanaka[2], Kenta Teruya[4], Katsumi Doh-ura[4], Ryuichi Sakai[5], Makoto Sasaki[6] and Masao Ikeda-Saito[2,3*]

[1]*Frontier Research Center for Applied Atomic Sciences, Ibaraki University, Tokai, Naka, Ibaraki 319-1106, Japan*
[2]*Institute of Multidisciplinary Research for Advanced Materials, Tohoku University, Katahira, Aoba, Sendai 980-8577, Japan*
[3]*RIKEN SPring-8 Center, Harima Institute, Sayo, Hyogo 679-5148, Japan*
[4]*Department of Neurochemistry, Tohoku University Graduate School of Medicine, Seiryo, Aoba, Sendai 980-8575, Japan*
[5]*Graduate School of Fisheries Sciences, Hokkaido University, Hakodate 041-8611, Japan*
[6]*Graduate School of Life Sciences, Tohoku University, Katahira, Aoba, Sendai 980-8577, Japan*

Received 18 April 2011;
received in revised form
11 August 2011;
accepted 23 August 2011
Available online
26 August 2011

Edited by R. Huber

Keywords:
gating efficacy;
discrimination;
ligand;
X-ray structure;
kainate-type ionotropic glutamate receptor

Dysiherbaine (DH) and neodysiherbaine A (NDH) selectively bind and activate two kainate-type ionotropic glutamate receptors, GluK1 and GluK2. The ligand-binding domains of human GluK1 and GluK2 were crystallized as bound forms with a series of DH analogues including DH, NDH, 8-deoxy-NDH, 9-deoxy-NDH and 8,9-dideoxy-NDH (MSVIII-19), isolated from natural sources or prepared by total synthesis. Since the DH analogues exhibit a wide range of binding affinities and agonist efficacies, it follows that the detailed analysis of crystal structure would provide us with a significant opportunity to elucidate structural factors responsible for selective binding and some aspects of gating efficacy. We found that differences in three amino acids (Thr503, Ser706 and Ser726 in GluK1 and Ala487, Asn690 and Thr710 in GluK2) in the ligand-binding pocket generate differences in the binding modes of NDH to GluK1 and GluK2. Furthermore, deletion of the C_9 hydroxy group in NDH alters the ligand conformation such that it is no longer suited for binding to the GluK1 ligand-binding pocket. In GluK2, NDH pushes and rotates the side chain of Asn690 (substituted for Ser706 in GluK1) and disrupts an interdomain hydrogen bond with Glu409. The present data support the idea that receptor selectivities of DH analogues resulted from the differences in the binding modes of the ligands in GluK1/GluK2 and the steric repulsion of

*Corresponding authors. M. Unno is to be contacted at Frontier Research Center for Applied Atomic Sciences, Ibaraki University, 169-1 Shirakata, Tokai, Naka, Ibaraki 319-1106, Japan; M. Ikeda-Saito, Institute of Multidisciplinary Research for Advanced Materials, Tohoku University, Katahira, Aoba, Sendai 980-8577, Japan. E-mail addresses: unno19@mx.ibaraki.ac.jp; mis2@tagen.tohoku.ac.jp.

Present address: K. Teruya, Department of Chemistry, Graduate School of Medical Science, Kyoto Prefectural University of Medicine, Kita-ku, Kyoto 603-8334, Japan.

Abbreviations used: AMPA, α-amino-3-hydroxy-5-methyl-4-isoxazolepropionate; a.u., asymmetric unit; DH, dysiherbaine; EDTA, ethylenediaminetetraacetic acid; iGluR, ionotropic glutamate receptor; KAR, kainate-type ionotropic glutamate receptor; MD, molecular dynamics; MSVIII-19, 8,9-dideoxy-NDH; NDH, neodysiherbaine A; PDB, Protein Data Bank; PEG, polyethylene glycol; s.g., space group.

Asn690 in GluK2. All ligands, regardless of agonist efficacy, induced full domain closure. Consequently, ligand efficacy and domain closure did not directly coincide with DH analogues and the kainate receptors.

Introduction

Ionotropic glutamate receptors (iGluRs) are synaptic receptors that form L-glutamate-gated ion channels and play central roles in excitatory neurotransmission in the mammalian central nervous system. Pharmacologically, iGluRs are classified into three broad subfamilies: *N*-methyl-D-aspartate (NMDA), α-amino-3-hydroxy-5-methyl-4-isoxazole-propionate (AMPA) and kainate-type ionotropic glutamate receptors (KARs).[1,2] The iGluR subfamily is composed of a total of 18 proteins. Isoforms within each subfamily assemble into homomeric or heteromeric oligomers in certain combination in order to form functional ion channels. Thus, functional synaptic receptors are highly diverse and inherently difficult to characterize.

Naturally occurring toxins represent valuable tools for neuropharmacological research, as they often selectively target neuronal receptors with high affinity, and they are able to modulate receptor function in unexpected ways. Dysiherbaine (DH) and neodysiherbaine A (NDH), isolated from the marine sponge *Lendenfeldia chondrodes*, provide a particularly interesting example of such a molecule. DH and NDH have been shown to be potent convulsants in mice and have been characterized as potent agonists for KARs.[3–5] DH has also been shown to bind selectively and to have unusually high affinity for both GluK1 (formerly known as GluR5) and GluK2 (GluR6) KAR isoforms and can selectively activate subunits in some heteromeric receptor complexes.[4,6] Thus, DH, NDH and their analogues may serve as interesting tools that characterize neuronal KARs in detail.[7–10]

Exploration of the structure–function relationships related to the function of DH analogues has yielded interesting and unexpected aspects of GluK1 and GluK2 KARs.[9,11,12] Structurally, DH and NDH contain a shared template, consisting of a *cis*-fused hexahydrofuro[3,2-*b*]pyran ring system with two functional groups at the C_8 and C_9 positions, in addition to a glutamate substructure (Fig. 1). Since relatively small differences in the functional groups at C_8 were found to impart significant effects upon binding affinity and selectivity as revealed by comparing the activity of DH and NDH, a series of NDH analogues including 8-deoxy-NDH, 9-deoxy-NDH and 8,9-dideoxy-NDH (MSVIII-19) was synthesized.[7,13] The binding affinities of these compounds for GluK1 and GluK2 are summarized in Table 1. For example, DH and NDH also bind strongly to GluK2, although 8-deoxy-NDH has a much lower affinity for GluK2 than those of DH and NDH. Furthermore, 9-deoxy-NDH and MSVIII-19 do not bind to GluK2.[11] These binding profiles are rather unexpected considering the structural similarity of both ligands and receptors, where GluK1 and GluK2 have 74% and 87% identity overall in terms of ligand-binding-core sequence identity, respectively.[15] Several functional aspects of the DH analogues are also intriguing. For example, it has been shown that DH, NDH and 8-deoxy-NDH are full or efficient agonists for GluK1, while 9-deoxy-NDH is only a partial agonist.[11] Moreover and of most interest is that MSVIII-19 acts as a

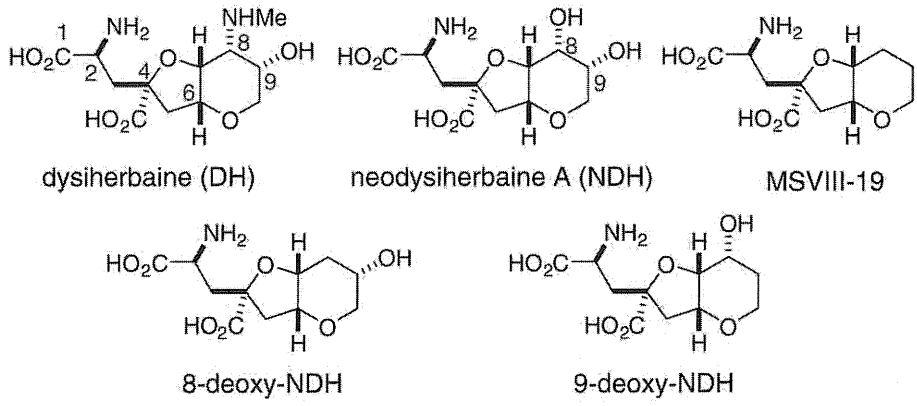

Fig. 1. Chemical structures of DH and its analogues.

Table 1. K_i values for displacement of [^{3}H]kainate by DH analogues[4,11,12,14]

K_i (nM)	L-glutamate	DH	NDH	MSVIII-19	8-deoxy-NDH	9-deoxy-NDH
GluK1	290	0.5	7.7	128	1.5	169
GluK2	1080	1.3	33	>100,000	48,000	>100,000

potential antagonist for GluK1.[12] Furthermore, MSVIII-19 induced a coma-like sleeping state in mice when administrated intracerebroventricularly, rather than induce convulsions. Recently, MSVIII-19 was also shown to exert analgesic properties in mice when applied intrathecally.[16] Collectively, these data indicated that although the structure–function relationships of DH analogues are complex, the polar functional groups at C_8 and C_9 play intriguing roles in the binding and gating of KARs. Recently, the crystal structures of rat GluK1 ligand-binding core (GluK1-S1S2) in complex with DH and MSVIII-19 were elucidated.[17] The structures showed that MSVIII-19 induced a full domain closure of GluK1-S1S2 instead of an "open" structure for the receptor in complex with an antagonist.[17] These results were contradictory to the previous proposal that antagonists stabilize an "open" rather than "closed" state of the receptor–ligand complex.[18–20] Accordingly, the gating properties of MSVIII-19 were further characterized at the pharmacological level and shown to induce gating current in only a very poor manner but desensitized the receptor effectively, thus acting as a functional antagonist.[16,17] It was thus concluded that, with GluK1, gating efficacy was not necessarily related to an agonist's ability to "close" the ligand-binding domain.[17]

These drastic changes in the mode of activity and isoform selectivity as a result of only a relatively small change in the functional group observed in NDH analogues are intriguing issues to explore further. Detailed analyses of the crystal structures of GluK1-S1S2 in complex with various NDH analogues with a wide range of binding affinities and agonist efficacies would further elucidate some of these interesting observations. Since we have developed a synthetic route that enables a relatively large supply of a series of DH analogues,[7,8,10] we conducted the crystallization of the human GluK1-S1S2 (hGluK1-S1S2) in complex with DH, NDH, MSVIII-19, 8-deoxy-NDH and 9-deoxy-NDH and obtained the structures at 1.5 Å resolution. In addition, we also obtained the structure of the hGluK1-S1S2 complex with L-glutamate at 1.65 Å resolution (Supporting Information, Table S1 and Fig. S1). Finally, we determined the crystal structure of the human GluK2-S1S2 (hGluK2-S1S2) in complex with NDH (Supporting Information and Table S1). In this paper, we describe detailed structures of the receptor–ligand complex, present a comparative view of structural implication in light of both receptor and ligand conformations and discuss differences in binding patterns arising from the structural alteration of the molecule.

Results

Overall structure

Amino acids are numbered with respect to mature proteins in accordance with the recommendations by Mayer,[21] and the corresponding residue numbers of preprocessed forms[17,22] are shown in parentheses.

The hGluK1-S1S2 crystals obtained during this study belonged to two different types of space groups (s.g.s): *C*2 and *P*1 (Supporting Information and Table S1). We obtained *P*1 crystals with high reproducibility in complex with L-glutamate, DH, NDH, MSVIII-19, 8-deoxy-NDH or 9-deoxy-NDH at up to 1.5 Å resolution (1.65 Å for L-glutamate) (Supporting Information and Fig. S1). However, *C*2 crystals were obtained for only the L-glutamate, DH and NDH complexes with very poor reproducibility. It is possible that the protein structures in *C*2 crystals may be an artifact (see Supporting Information for details). Comparisons of *P*1 and *C*2 crystals are also described in Supporting Information. We thus utilized molecules from *P*1 crystals as hGluK1-S1S2 throughout the discussion.

The hGluK1-S1S2 monomer has two subdomains, namely, domain 1 [residues 420–520 (435–535) and residues 747–786 (762–801)] and domain 2 [residues 521–746 (536–761)], as depicted in Fig. 2a. Each ligand was located between domain 1 and domain 2. The overall structures of hGluK1-S1S2s monomers are essentially the same, irrespective of bound ligands [C^α root-mean-square (r.m.s.) differences are 0.1–0.40 Å]. The monomer of hGluK1-S1S2 interacts with the other monomer in a dominant manner via domain 1 (Fig. 2b). The intermolecular varied area was 7226 Å^2. One monomer can be generated by reflecting a plane and rotating approximately 80° against the other monomer (Fig. 2b). The structures of the two monomers are essentially the same with a C^α r.m.s. difference of 0.35 Å.

Crystals of hGluK2-S1S2 were obtained in complex with NDH, belonging to s.g. $P2_1$, and contained two molecules in its asymmetric unit (a.u.). Structure was determined at 1.65 Å resolution (Supporting Information and Table S1). The monomer structure was similar to that of the hGluK1-S1S2–NDH

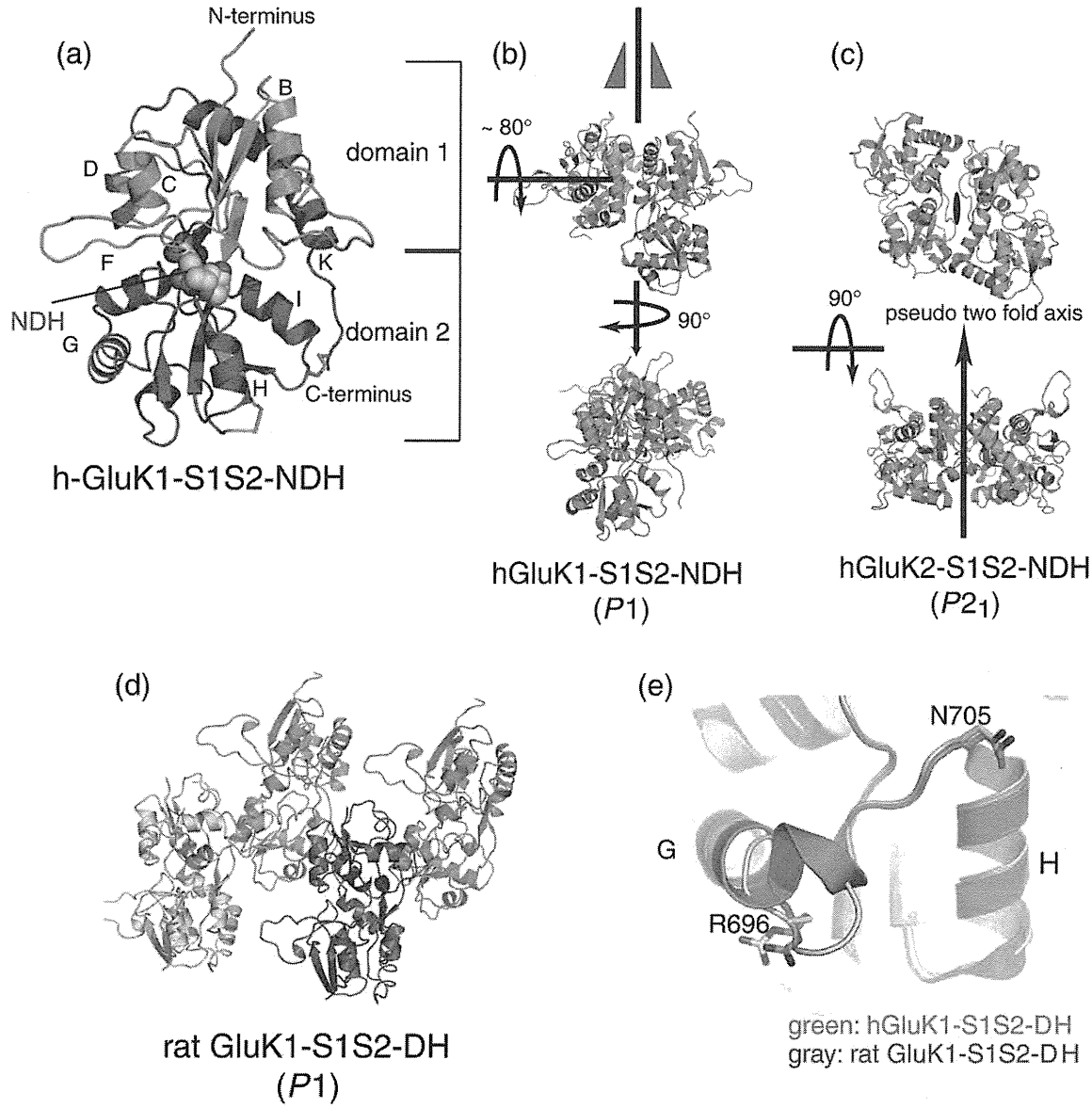

Fig. 2. The overall structure of hGluK1-S1S2 in complex with NDH. (a) S1 and S2 segments are shown in green and magenta, respectively. NDH is depicted by the CPK model (C, N and O atoms are represented as yellow, blue and red, respectively). Initials represent α-helices, which are named in accordance with Mayer's recommendations.[21] (b) hGluK1-S1S2 monomer–monomer interaction in *P*1 crystals and (c) monomer–monomer interaction in hGluK2-S1S2, viewed from two directions. Monomers are depicted in green and cyan. (d) Four molecules of rat GluK1-S1S2 in the a.u. Monomers are depicted in green, cyan, magenta and yellow. Intermolecular interactions are quite different from those in human. (e) Superposition of hGluK1-S1S2 (green) and rat GluK1-S1S2 (gray).

complex with a C^{α} r.m.s. difference of 0.85 Å and was essentially the same as that of the rat GluK2-S1S2 L-glutamate complex reported previously[21] with a C^{α} r.m.s. difference of 0.60 Å.

The hGluK2-S1S2 monomer interacts with the other monomer in a head-to-tail fashion (Fig. 2c). The intermolecular interaction is quite different from that found in the hGluK1-S1S2 in the *P*1 crystals. The intermolecular varied area was 6893 $Å^2$. One monomer can be generated by rotation against a pseudo-2-fold axis (Fig. 2c). The C^{α} r.m.s. difference between the two monomers was 0.29 Å.

The clear differences in the dimer structure between hGluK1-S1S2 and hGluK2-S1S2 imply that the ligand-binding core of KARs should be considered as a monomer, as highlighted by Frydenvang *et al.*[17]

Comparative structural analysis with reference to DH and MSVIII-19 complex structures reported previously

Frydenvang *et al.* previously reported crystal structures for rat GluK1-S1S2 in complex with DH and MSVIII-19.[17] Since three residues, Leu463 (478), Ser700 (715) and Lys704 (719) and Ile463 (478), Thr700 (715) and Arg704 (719), in the ligand-binding core of rat and human, respectively, are different and since the crystallization conditions employed were not identical between existing studies, we decided

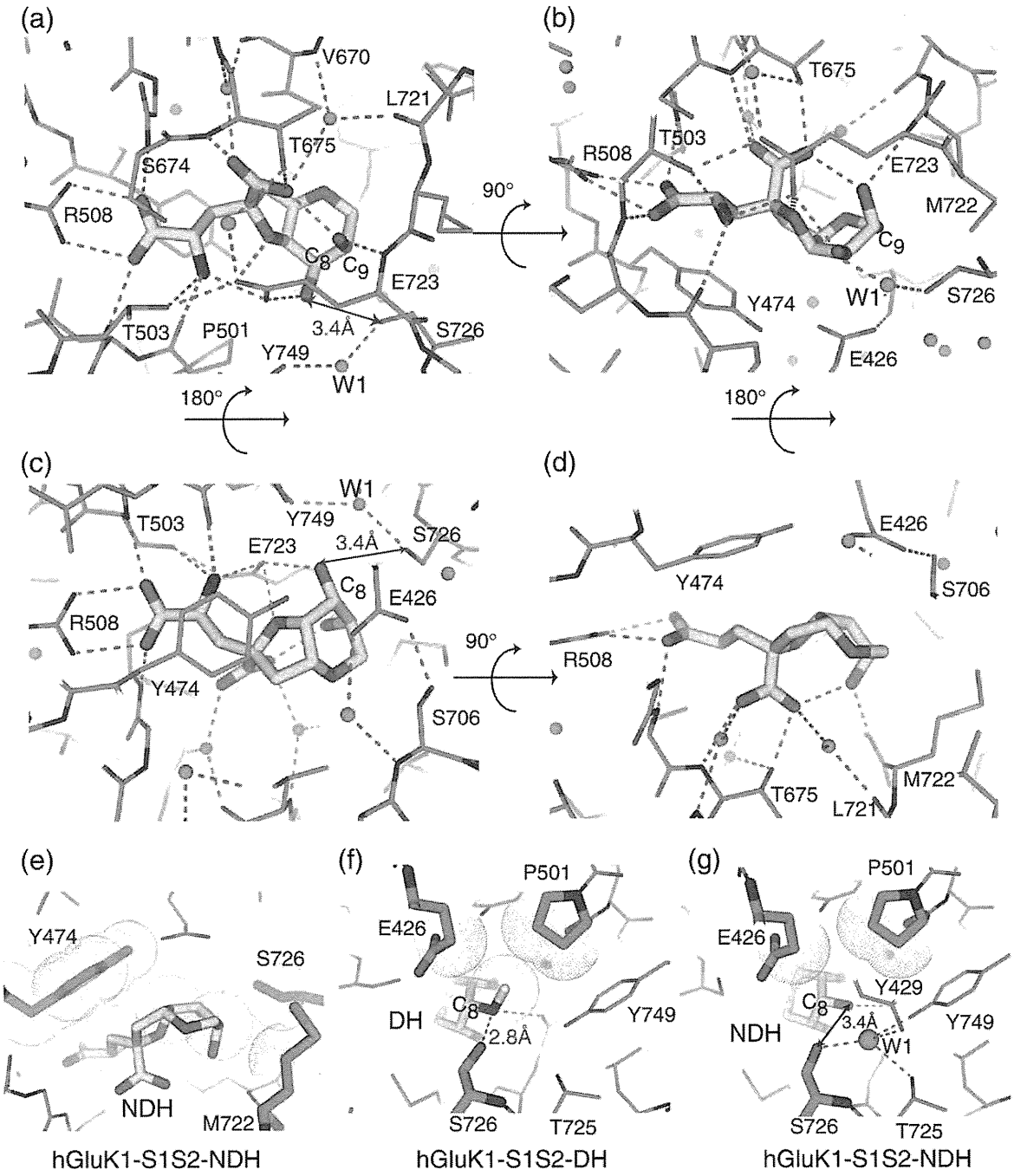

Fig. 3. Modes of ligand binding in hGluK1-S1S2. (a–d) Hydrogen-bonding interactions between NDH and surrounding residues from four directions. Cyan balls represent water molecules. (e) van der Waals contacts between NDH and GluK1 ligand-binding domain. (f) van der Waals contacts and hydrogen-bonding interactions between the DH *N*-methylamino group and GluK1. (g) van der Waals contacts in the hGluK1-S1S2–NDH complex. The cyan ball indicates the nearby water molecule, which is found only in the NDH complex.

Table 2. Hydrogen-bonding interactions between NDH and hGluK1-S1S2 and between NDH and hGluK2-S1S2 (average distances of two molecules in the a.u.)

NDH	hGluK1-S1S2	Average distance (Å)	hGluK2-S1S2	Average distance (Å)
C_8OH	Glu723O$^{\varepsilon 1}$	2.79	Glu707O$^{\varepsilon 1}$	2.91
C_8OH	—	—	Thr710OH	2.66
C_9OH	Glu723N	2.78	Glu707N	2.78
Five-membered ring O	Glu723O$^{\varepsilon 1}$	3.04	Glu707O$^{\varepsilon 1}$	3.18
Six-membered ring O	—	—	Water 1	3.14
Glutamate O1	Thr503N	2.85	Ala488N	2.87
Glutamate O1	Arg508N$^{\eta 1}$	2.83	Arg493N$^{\eta 1}$	2.86
Glutamate O2	Arg508N$^{\eta 2}$	2.77	Arg493N$^{\eta 2}$	2.71
Glutamate O2	Ser674N	2.78	Ala658N	2.79
Glutamate N	Thr503OH	2.92	—	—
Glutamate N	Glu723O$^{\varepsilon 1}$	2.83	Glu707O$^{\varepsilon 1}$	2.76
Glutamate N	Pro501O	2.86	Pro486O	2.85
Glutamate γ-carboxylate OAA	Thr675OH	2.67	Thr659OH	2.60
Glutamate γ-carboxylate OAA	Water 1	3.19	—	—
Glutamate γ-carboxylate OAE	Thr675N	3.05	Thr659N	3.03
Glutamate γ-carboxylate OAE	Water 2	2.86	Water 2	2.67

first to carry out a detailed analysis of the structure. Crystals of rat GluK1-S1S2 in complex with DH belonged to s.g. *P*1 and contained four monomers in the a.u.,[17] whereas the human counterpart contained just two monomers (Fig. 2b and d). Overall, the monomer structures of rat and human DH complexes were quite similar, except for a few residues in the N-terminal region and some flexible loops. The overall C^{α} r.m.s. difference was 0.99 Å. DH-binding regions were similar. We identified two conformations of the Tyr429 (444) side chain in our present structure, while only a single conformation was observed in the rat counterpart (Supporting Information and Fig. S3). However, the importance of these Tyr429 (444) conformations remains unclear. The largest differences in structure were detected in the loop conformation between helix G and helix H [between Arg696 (711) and Asn705 (720)] (Fig. 2e). Only these two points can be considered as salient differences between the two structures. All other structural aspects remain almost identical. The DH-binding mode remained essentially the same.

The crystal of hGluK1-S1S2 in complex with MSVIII-19 belonged to s.g. *P*1 and contained two monomers in the a.u. as reported previously for the rat MSVIII-19 complex.[17] Overall, monomer structures of human and rat MSVIII-19 complexes were similar apart from a flexible loop between Arg696 (711) and Asn705 (720). The overall C^{α} r.m.s. difference was 1.01 Å. Thus, the structures of MSVIII-19-binding regions and its binding mode in human and rat receptors can be considered to be essentially the same (*vide infra*). The Tyr429 (444) side chain exhibited a single conformation.

Binding mode of NDH in hGluK1-S1S2

NDH was shown to bind to the ligand-binding pocket of hGluK1-S1S2 in a manner similar to that observed with DH. The bulky bicyclic portion of the ligand expelled four water molecules originally found in the L-glutamate complex,[21,22] enabling direct hydrogen-bonding interaction with the protein (Fig. 3a–d and Table 2). van der Waals interactions between the C_5, C_7 and C_8 atoms in the bicyclic portion with Tyr474 (489), Met722 (737)C^{γ} or Ser726 (741)C^{β} were also present in the NDH complex, in which the C–C distance was between 3.4 and 4.1 Å (Fig. 3e).

The role of C_8 functional groups in the GluK1-S1S2 ligand-binding pocket

As previously reported, in the DH complex, the C_8 *N*-methylamino group engaged in van der Waals interactions with Glu426 (441)C^{γ}, Pro501 (516)C^{β} and Pro501 (516)C^{γ} (Fig. 3f).[17] In addition, hydrogen-bonding interactions were formed between the C_8 *N*-methylamino group and Ser726 (741)OH (Fig. 3f). Molecular dynamics

Fig. 4. Differences in the three-dimensional structure between 9-deoxy-NDH and NDH bound to hGluK1-S1S2. (a) The structure of NDH; (b) the structure of 9-deoxy-NDH. (c) Modeled 9-deoxy-NDH fitting the $F_o - F_c$ electron density map contoured at 3.0-σ level calculated without 9-deoxy-NDH viewed from two directions. (d) 9-Deoxy-NDH shows loss of van der Waals contacts with Glu426 (441). (e) Superposition of 9-deoxy-NDH (yellow-based) and MSVIII-19 (gray-based). Numbers written in magenta represent carbon atoms in 9-deoxy-NDH, while those written in black are carbon atoms in MSVIII-19. (f) 9-Deoxy-NDH shows double conformations, predominantly in a twisted-boat form but also partly in an extended chair form. Vivid yellow represents the major conformation in a twisted-boat form, which is refined with occupancy at 0.6. Lime and pink represent the minor conformation in a chair form, which is refined with occupancy at 0.4. The latter is very similar to the structure of MSVIII-19. The main chain is modeled in single conformation.

(MD) simulation results suggested that hydrogen bonding may represent a key factor underlying the pharmacological specificity of DH.[23] Furthermore, the C_8 *N*-methylamino group of DH is stabilized by hydrogen-bonding interactions with Glu723 (738) carboxylate. All such interactions

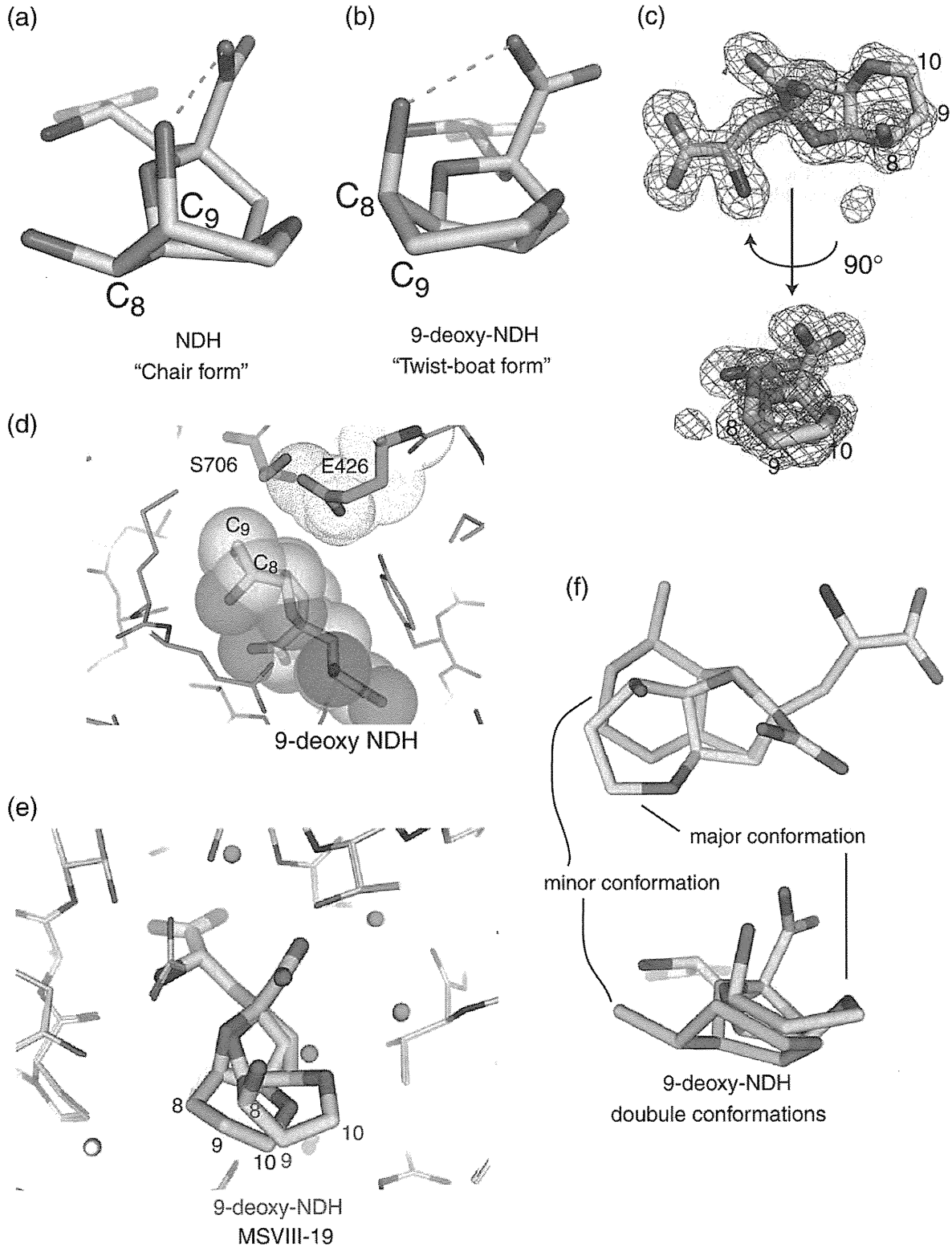

Fig. 4 (*legend on previous page*)

were reproduced in the hGluK1-S1S2–DH complex (Fig. 3f).

In the case of NDH, the conformations of both ligand and the surrounding residues might change slightly, compared to those of the DH complex. This is due to the differences in the C_8 functional groups when DH and NDH are compared. In the NDH complex, we observed that the distance between the C_8 hydroxy group and Ser726 (741)OH was 3.4 Å, which is too far to allow effective hydrogen-bonding interaction (Fig. 3a, c and g). A lack of a methyl group at the oxygen atom at C_8 in NDH excludes the stabilizing effect of van der Waals interactions (Fig. 3g), which were observed in the DH complex (Fig. 3f). Thus, the difference in the C_8 functionality may explain the lower affinity of NDH for GluK1 as compared to that of DH (Table 1).

In addition, we observed a water molecule (W1) that intervenes between the C_8 hydroxy group and the protein matrix in the NDH complex (Fig. 3). This water molecule was stabilized by Tyr429 (444)OH, Thr725 (740)OH, Ser726 (741)OH and Tyr749 (764) OH with hydrogen bonds (Fig. 3g). Although interatomic distance between the C_8 hydroxy group of NDH and W1 (3.0 Å) may allow the formation of hydrogen bonds, its contribution in stabilizing the complex is likely to be negligible since the affinity of 8-deoxy-NDH for GluK1 is comparable with that of NDH (Table 1). Of particular note, W1 was indeed found in the structure of the 8-deoxy-NDH complex (Supporting Information and Fig. S1) as well but not in the DH complex (Fig. 3f).

Importance of the C_9 hydroxy group in NDH analogues for the protein–ligand complex stability

In the crystal structures of DH, NDH and 8-deoxy-NDH bound to hGluK1-S1S2, distances between the C_9 hydroxy group and the γ-carboxylate within the glutamate substructure were within 2.9 Å, suggesting the presence of hydrogen-bonding interaction between them (Fig. 4a). This peculiar intramolecular interaction resulted in these ligand molecules exhibiting highly folded conformations. In contrast, MSVIII-19 did not exhibit such interactions since it lacked a C_9 hydroxy group, as reported previously.[17] Unexpectedly, however, we found that a major conformer of 9-deoxy-NDH in complex with GluK1 formed an intramolecular hydrogen bond between its C_8 hydroxy group and the γ-carboxylate of the glutamate substructure, rather than the C_9 hydroxy group. Consequently, the tetrahydropyran ring of 9-deoxy-NDH predominantly exists in a twisted-boat form (Fig. 4b and c). Owing to this distorted boat conformation, the van der Waals interaction between the tetrahydropyran ring and Glu426 (441)C^{δ} is lost (Fig. 4d). The C_9 atom of 9-deoxy-NDH is positioned at almost the same point as the C_{10} atom of MSVIII-19 when superimposed (Fig. 4e). Interestingly, a minor conformer that lacks a hydrogen bond with the γ-carboxylate was also found in the electron density map (Fig. 4c and f). Collectively, these results indicated that the C_9 hydroxy group of NDH analogues represents a key functional group not only for forming hydrogen-bonding interaction with Glu723 (738) main-chain amide (Fig. 3a and b) but also for maintaining the unique conformation by the intramolecular hydrogen bond with the γ-carboxylate (Fig. 4a).

Differences in NDH-binding modes in GluK1 and GluK2

Ligand-binding-core structures of human GluK1 and GluK2 are very similar and share 87% sequence identity. However, GluK1 possesses a binding cavity larger than that of GluK2,[21] and ligand binding to GluK2 is generally less favorable than that to GluK1.[21,24] As Lash *et al.* have reported previously, GluK1/GluK2 selectivity differs significantly among the NDH analogues, although the size of these molecules does not differ drastically.[11] Thus, the crystal structures obtained in this study for the NDH complex with GluK2 are likely to provide us with significant insight into the associated binding properties.

The crystal structures of NDH complexes with GluK1 and GluK2 were similar, but intriguing differences in some binding profiles were observed between NDH-bound GluK1 and GluK2. These differences were analogous to the L-glutamate-bound structures of GluK1 and GluK2.[21] Thr503 (518) in GluK1 formed two hydrogen bonds between the α-amino group of NDH and the δ-carboxylate of Glu723 (738) (Fig. 5a), whereas a lack of direct hydrogen bonding with the corresponding residue Ala487 (518) in GluK2 resulted in a slight change in conformation and orientation at Glu707 (738) (Fig. 5b). The C^{α}–C^{β} axis of Glu707 (738) in GluK2 was tilted by ~10° compared to that of Glu723 (738) in GluK1. The orientation and conformation of NDH were also different in both receptors. The glutamate substructure of NDH was tilted by 5°, and the bulky bicyclic portion of NDH in GluK2 was rotated about 10° around the C_3–C_4 axis. These differences induced a shift in their positions by approximately 1.0 Å (Fig. 5c).

In GluK1, a water molecule (W1) was found in close proximity to the C_8 hydroxy group of NDH. The distance between Ser726 (741)OH and the C_8 hydroxy group was 3.4 Å (Figs. 3a and c and 5a). These data suggest that a direct hydrogen bond between the C_8 hydroxy group of NDH and Ser726 (741)OH in GluK1 is not effective (*vide supra*). However, in the case of GluK2, Thr710 (741), which corresponds to Ser726 (741) in GluK1, can form direct hydrogen bonds with the C_8 hydroxy group

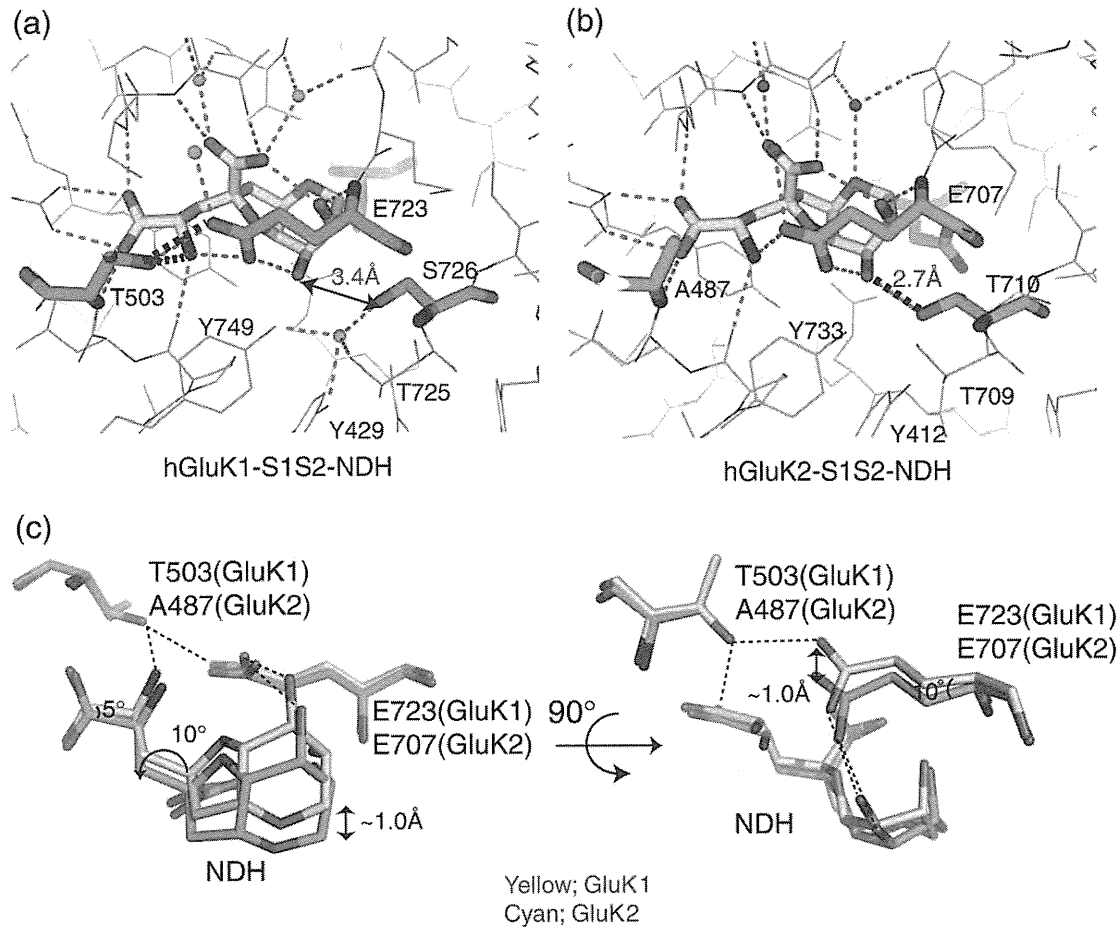

Fig. 5. Differences in the modes of NDH binding in GluK1 and GluK2. (a) NDH in GluK1. (b) NDH in GluK2. (c) Structural displacement of NDH and the nearby glutamate. The yellow-based figure is in GluK1, and the cyan-based figure is in GluK2. Pictures from the two point of views are depicted in order to clarify the conformation and orientation changes in NDH and the nearby glutamate.

of NDH, a feature attributable to their closer proximity (2.7 Å) (Fig. 5b). Moreover, the proximity between other proton donors and acceptors within the bicyclic portion of NDH and the protein matrix in GluK1 and GluK2 is different (summarized in Table 2). Consequently, the hydrogen-bonding network formed between NDH and GluK1 or GluK2 might be one of the factors that differentiate the binding affinity of NDH to the receptors (see Discussion).

Conformation of Asn690 in GluK2

The most significant difference identified in the structure of the hGluK2-S1S2–NDH complex, when compared to the L-glutamate complex [Protein Data Bank (PDB) ID 1S50][21] or the kainate complex (PDB ID 1TT1)[21] of GluK2, was the conformation of Asn690 (721). In the structure of rat GluK2-S1S2 in complex with L-glutamate or kainate, the side chain of Asn690 (721) points toward the bound ligands (Fig. 6a and b). In contrast, in the NDH complex, Asn690 (721) points away from the ligand due to steric hindrance between the side chain and the six-membered ring of NDH (Fig. 6c). This rather drastic conformational change in Asn690 (721) resulted in disruption of the hydrogen bond between Glu409 (441) and Asn690 (721). The distance between Glu409 (441)$O^{\varepsilon 2}$ and Asn690 (721)$N^{\delta 2}$ was 3.9 Å, and the angle Glu409 (441)$O^{\varepsilon 2}$–Asn690 (721)$N^{\delta 2}$–Asn690 (721)C^{γ} was 75°, which is too far and too acute to form hydrogen bonds. These data suggest that NDH binding forced rotation of the Asn690 side chain, which is not required in smaller ligands such as L-glutamate and kainate (Fig. 6a and b). The corresponding Ser706 (721) conformation in hGluK1-S1S2–NDH did not differ from that seen in the L-glutamate complex of GluK1 because serine is smaller than asparagine [Asn690 (721) in GluK2], and thus, NDH can bind to the GluK1 ligand-binding pocket without conformational change (Fig. 6d).